Astron. Astrophys. 362, 465–586 (2000)

ASTRONOMY AND ASTROPHYSICS

N-body simulations of resonance rings in galactic disks

P. Rautiainen and H. Salo

University of Oulu, Department of Physical Sciences, Division of Astronomy, P.O. Box 3000, 90014 Oulun yliopisto, Finland

Received 16 February 2000 / Accepted 14 August 2000

Abstract. We have studied the formation of rings in the disks of galaxies by using two-dimensional N-body simulations where the gas component is modelled as dissipatively colliding test particles. Our results support the standard hypothesis that ring formation occurs when gas is driven to resonances by the gravitational torque of a rotating stellar bar. When the bar is absent, a weaker oval-shaped mode or a spiral mode can have the same effect. Typical locations of the rings are as follows: the outer rings are usually near the outer Lindblad resonances, the inner rings near the inner 4/1-resonance and the nuclear rings near the inner Lindblad resonances. However, we have also found a few exceptions to these rules.

We also have studied why a significant fraction of barred galaxies lack one, two or all ring types. Our models suggest that the absence of rings may be related to timescales of ring formation: the inner and nuclear rings usually form faster than the outer rings. The lack of inner and nuclear rings can be related to the strength of the bar: in high amplitude cases, one or both of these ring types are absent. Also, bars may rotate fast enough such that they lack the inner Lindblad resonance and thus cannot form nuclear rings.

The potential outer ring region is often dominated by a slower spiral mode, which in principle could inhibit or delay ring formation. However, we found that when both the bar mode and the slower spiral mode coexist in the outer disk, there can be almost cyclic alternation between different outer ring morphologies. In addition to the outer Lindblad resonance of the bar, certain resonances of the slower mode can also exist near the ring radius. The deceleration of the bar rotation rate and the corresponding change in the resonance positions did not inhibit ring formation or destroy an existing ring. The presence of more than one mode could also affect the region of inner or nuclear rings. This can explain part of the case in which the ring is misaligned with respect to the main bar component.

Key words: galaxies: evolution – galaxies: fundamental parameters – galaxies: kinematics and dynamics – galaxies: spiral – galaxies: structure

Send offprint requests to: P. Rautiainen (pertti.rautiainen@oulu.fi)

1. Introduction

Many galaxies have rings in their disks. These rings are probably the result of the internal evolution of their host systems, which are sometimes called ringed galaxies. When we speak of rings in this article, we mean this specific type of ring, not the so-called ring galaxies or the polar ring galaxies, which are likely created by interactions between galaxies (see e.g. Athanassoula & Bosma 1985).

Although rings are also found in non-barred galaxies, they are more common in barred systems (Buta & Combes 1996). It is generally accepted that the rings are located near resonances, which are induced by a bar or an oval component. It is thought that the gravitational torque of a rotating stellar bar drives interstellar gas into regions where the orbits of gas clouds are aligned either parallel or perpendicular to the bar major axis, and thus the net torque vanishes. In non-barred galaxies the rings may be related to resonances induced by a spiral mode or could be relics formed by a dissolved bar. It is also known that many apparently non-barred galaxies have a hidden bar or oval component that can be seen in near-IR (see e.g. Zaritsky & Lo 1986).

Rings are divided to outer, inner and nuclear rings based on their sizes relative to the bar. The major axes of the outer rings (R) and the pseudorings (R') are about twice that of the bar, the major axes of the inner rings (r) are usually filled by the bar and in the case of nuclear rings (nr), the major axes are about 1/10 of the bar major axis. There are two subclasses of outer rings and pseudorings; in the R_1 and R'_1 subclass, the major axis of the ring is perpendicular to the bar and in the R'_2 subclass it is parallel to the bar. R'_1 pseudorings often have dimples near the ends of the bar. Complete detached outer rings can have similar features and thus also will be classified as R_1, but usually it is impossible to apply subclasses to complete outer rings. There is also a combined outer ring morphology $R_1R'_2$ (Buta & Crocker 1991; Buta 1995; Buta & Combes 1996).

The connection between inner rings and bars seems evident, although sometimes the bar ends before reaching the inner ring, and there are few galaxies where these structures are misaligned (Buta et al. 1995b). The inner rings are usually thought to be related to the inner 4/1-resonance of the bar. The situation with nuclear and outer rings is less clear. Although the nuclear rings are usually close to the deduced positions of the inner Lindblad res-

onance (ILR), they do not have clearly preferred position angles relative to the bar and it is possible that several of them are related to nuclear bars rather than the main bar component (Friedli & Martinet 1993; Buta & Crocker 1993). The shapes of the two subclasses of outer rings fit well to the shapes of the orbit families near the outer Lindblad resonance (OLR), but it has been stressed that the absence of outer rings in many barred galaxies also requires an explanation (see e.g. Sellwood & Wilkinson 1993). Furthermore, in many self-gravitating simulations, there is more than one mode present (Sellwood & Sparke 1988; Masset & Tagger 1997; Rautiainen & Salo 1999): the outer disk can be dominated by a mode that has a lower pattern speed than that of the bar. Intuitively, one would expect that in such situation, the outer ring would not form in the vicinity of the OLR of the bar. On the other, if the difference of pattern speeds of the outer disk and the bar is a typical situation, it is hard to understand why there are two subclasses of outer rings, differing by their orientation relative to the bar.

The previous studies of ring formation in barred galaxies (Schwarz 1981; Combes & Gerin 1985; Byrd et al. 1994; Piner et al. 1995) have used analytical two-dimensional rigidly rotating bar potential models. These studies are less realistic than N-body simulations, where the characteristics of the bar and the spiral arms are not arbitrary, but are determined by the initial stage of the systems. More realistic models can be constructed by deriving the potential from near-IR observations (e.g. Lindblad et al. 1996). This has been done for a few individual ringed galaxies, IC 4214 (Salo et al. 1999), ESO 565-11 (Buta et al. 1999b), and NGC 1433, NGC 3081 and NGC 6300 (Buta & Combes 2000). However, even these studies are inferior to N-body simulations because they model only the present stage of these systems, but do not reach their evolution. Moreover, these studies assume that a single mode dominates throughout the system. On the other hand, in most N-body studies on barred galaxies, only little attention has been paid to ring formation. Here our goal is to fill this gap by asking what modifications the N-body simulations (especially the possible presence of several simultaneous modes) can introduce to the ring formation process. We do not try to model any particular galaxy, but will frequently make qualitative comparisons with observations. In doing this, the Catalog of Southern Ringed Galaxies, CSRG (Buta 1995), has been most useful.

In the next section we describe the methods we have applied. We then present and analyse our simulation models. Finally, we discuss the relation between our simulations and observations.

2. Methods

We made N-body simulations with a self-gravitating stellar disk by using a two-dimensional logarithmic polar grid to calculate the potential. Typical grid geometry is 144 radial and 108 azimuthal cells. We also reproduced a few of our models with a 3-fold higher grid resolution to check the possible effects of grid softening. The standard particle number in our simulations was 500 000, distributed as an exponential disk with a cut-off radius at six disk scale lengths. Here we adopt a scaling where the scale length of the disk equals to 3 kpc. To test the effect of particle number we repeated some of the models with 200 000 and 1 000 000 particles. The value of the softening parameter was 1/8 of the disk scale length. The initial velocity distribution was created using the epicyclic approximation and corrected for asymmetric drift. The movement of particles was integrated by the time-centred leap-frog method for a time span corresponding to 15 gigayears. The length of a time step was 250 000 years, corresponding about 150 time steps per rotation period at the distance of one disk scale length, and to about 40 time steps very near the centre.

The gas component was modelled by inelastically colliding massless test particles. In each impact, the normal component of the relative velocity of the colliding particles was reduced to zero, i.e. the so-called coefficient of restitution α is set to 0.0. On the other hand, the tangential component of the relative velocity was retained. In most simulations 20 000 particles were used, having a uniform surface density to the outer edge of the stellar disk. The usual value of the particle radius is 7.5 pc. This yields a collision frequency from 20 to 400 per particle during one gigayear. The lowest value is for systems before the formation of a bar or a global spiral structure and the highest for systems with strong bars and nuclear rings. Similar treatment of the gas component was used in Salo (1991), Byrd et al. (1994) and Salo et al. (1999).

We have followed the evolution of our models by classifying the ring structures and by measuring their major and minor axes. In addition to morphological analysis, we have studied the Fourier decomposition of disk surface density:

$$\Sigma(r,\theta) = \Sigma_0(r)\left[1 + \sum_{m=1}^{\infty} A_{\rm m}(r)\cos\left(m(\theta - \theta_{\rm m}(r))\right)\right], \quad (1)$$

where r and θ are the polar coordinates, $\Sigma(r,\theta)$ the disk surface density, Σ_0 the axisymmetric surface density and $A_{\rm m}(r)$ and $\theta_{\rm m}(r)$ are the Fourier amplitude and phase angles. This decomposition was done separately for the stellar and the gas components by 200 times per Gyr. From the temporal evolution of $A_{\rm m}(r)$ and $\theta_{\rm m}(r)$ we constructed amplitude spectra (see e.g. Masset & Tagger 1997) $W_{\rm m}(r,t)$ displaying the amplitude of signals at different pattern speeds and distances. This gave essential information about the evolution of the system, especially when several modes were present. The resonance radii were determined by plotting curves showing $\Omega_{\rm c}$ and $\Omega_{\rm c} \pm \kappa/m$ with the amplitude spectra and measuring where the modes crossed these curves. Here $\Omega_{\rm c}$ and κ are the circular and epicycle frequencies, respectively. The most important resonances are the Lindblad resonances ($m = 2$), the ultraharmonic ($m = 4$) or 4/1-resonances and the corotation resonance, where the pattern speed of the mode is equal to local circular frequency. These resonance radii were then compared with the sizes of the rings in selected timesteps. The amplitude spectra of the gas component were used to confirm whether the gas in the rings follows the modes of the stellar component or not. We do not include the amplitude spectra of the gas component in this article for two reasons: to limit the number of figures and because these spectra are very noisy due to small particle number.

We also used the Fourier decompositions to determine the timescales of bar and ring formation more accurately: due to computer disk space limitations, the particle positions were saved only by every 625 million years, which is not always accurate enough. On the other hand, the higher saving frequency of the Fourier decompositions makes more accurate timescale estimates possible. We compared the morphologies of the particle position images with those constructed from the Fourier components, and found that they give equivalent gas morphology. The spiral structure of the stellar component was often better resolved in the images constructed from the Fourier components. We noticed that certain relative orientation of bar and spiral modes with different pattern speeds can give a temporary illusion of a considerably longer bar component than the actual one. A similar phenomenon was also found by Debattista & Sellwood (2000).

In a few selected models, we inferred the actual shapes of the modes by the method we applied in Rautiainen & Salo (1999): first, we rotated the Fourier phase angles of the decomposition of Eq. 1 to a coordinate system rotating with the same angular speed as the mode (measured from the amplitude spectrum), we then constructed the $m = 2$ component of the density distribution from the Fourier decomposition, and finally we summed and averaged the images into a single image showing the actual shape of the mode. Naturally, this method can be applied only when the pattern speed and the shape do not change much during the time interval used. Basically, the reconstructed images of the modes can include ghost images produced by other modes. To ensure that these do not interfere with our images, we checked the amplitude levels of the ghost images and found them to be below the lowest displayed contour level.

We have also studied the velocity dispersion of the gas component in our models. We did this by measuring the local radial velocity dispersion in a grid with 100 by 100 cells covering the disk. In calculating the average radial velocity dispersion we included the data only from the grid cells with at least ten particles.

3. Simulations

We performed self-consistent simulations with a wide range of initial parameters. When compared to models which use rigid bar potentials, these simulations provide new elements, especially concerning the long-term evolution of the system and the possibility of more than one mode being present in the disk (e.g. Sellwood & Sparke 1988; Rautiainen & Salo 1999).

We studied three basic families of mass models, each producing a fairly similar initial rotation curve in the inner parts of the disk. In family A the rotation curve is disk dominated, except in the central area where the bulge dominates. Family B has a strong halo and the rotation curve is dominated by the spheroidal component (including both the halo and the bulge), except in a small area where the disk provides an equal contribution. Family C is a mixture where the halo starts to dominate only in the outer disk. The rotation curves of these models are shown in Fig. 1.

In all models, the bulge component was modelled as an analytical Plummer sphere. The bulge scale length is 0.6 kpc and mass is 1.6×10^{10} $\mathrm{M}_\odot$. We also performed simulations where we changed the bulge scale length to 7.5 kpc to produce a more slowly rising rotation curve (these models are denoted by the superscript ' in the following paragraphs). The disks are exponential disks with scale lengths of 3 kpc and a cut-off radius of six scale lengths. In families A and C (and also in A' and C'), the disk mass is 7.5×10^{10} $\mathrm{M}_\odot$, and in family B (and B') it is 4.8×10^{10} $\mathrm{M}_\odot$. In model families B and C (and B' and C') we use an analytical halo potential, which is an isothermal sphere with a smooth transition to a constant core density. Inside five disk scale lengths, the halo mass in family B is 6.0×10^{10} $\mathrm{M}_\odot$ and in family C is 5.3×10^{10} $\mathrm{M}_\odot$.

One of the most important initial parameters that determines the further evolution of the models is the Toomre parameter (Toomre 1964):

$$Q_\mathrm{T} = \frac{\sigma_\mathrm{R}\kappa}{3.36G\Sigma}, \qquad (2)$$

where σ_R is the radial velocity dispersion of the disk, κ the epicycle frequency, G the constant of gravity and Σ the disk surface density. Although the value of $Q_\mathrm{T} > 1$ is enough to stabilise the disk against local axisymmetric instabilities, values typically larger than two are required to inhibit bar formation (see e.g. Athanassoula & Sellwood 1986). We carried out simulations with several values of the Toomre parameter from 1.25 to 2.5, for different degrees of halo-to-disk mass-ratio. Note that in simulations with softened gravity, the value of the softening parameter also affects the stability properties. Thus, the effective value of the Toomre parameter is higher than that implied by Q_T (Romeo 1994). One should also note that since we use epicycle approximation in the construction of the initial state, the models with the highest values of Q_T are a bit problematic: although they can avoid bar instability, they can suffer considerable mass redistribution in their early evolution.

3.1. Disk dominated models

Fig. 2 shows the amplitude spectra of the stellar component for four different simulations using the disk dominated mass model A. The values of Q_T are 1.25, 1.75, 2.25 and 2.5. The corresponding morphologies of the stellar and gas components are shown in Fig. 3. For both the stellar and gas components, the densities are indicated as shades of grey (in a logarithmic scale) in the same frames, but the gas number density was multiplied by twenty for clarity. The effect of the Toomre parameter is clear. Bar formation occurs faster in the models with a cooler initial disk, in agreement with previous studies (see e.g. Athanassoula & Sellwood 1986).

In the simulation with $Q_\mathrm{T} = 1.25$ (hereafter model A1.25) bar forms very quickly, by $T = 0.5$ Gyr. This bar mode has a spiral component with the same pattern speed, and there are also two spiral modes with lower pattern speeds. Later, the middle mode weakens but the outer mode becomes stronger. The amplitude spectrum suggests that there could be a nonlinear coupling between the bar and the stronger spiral mode such that

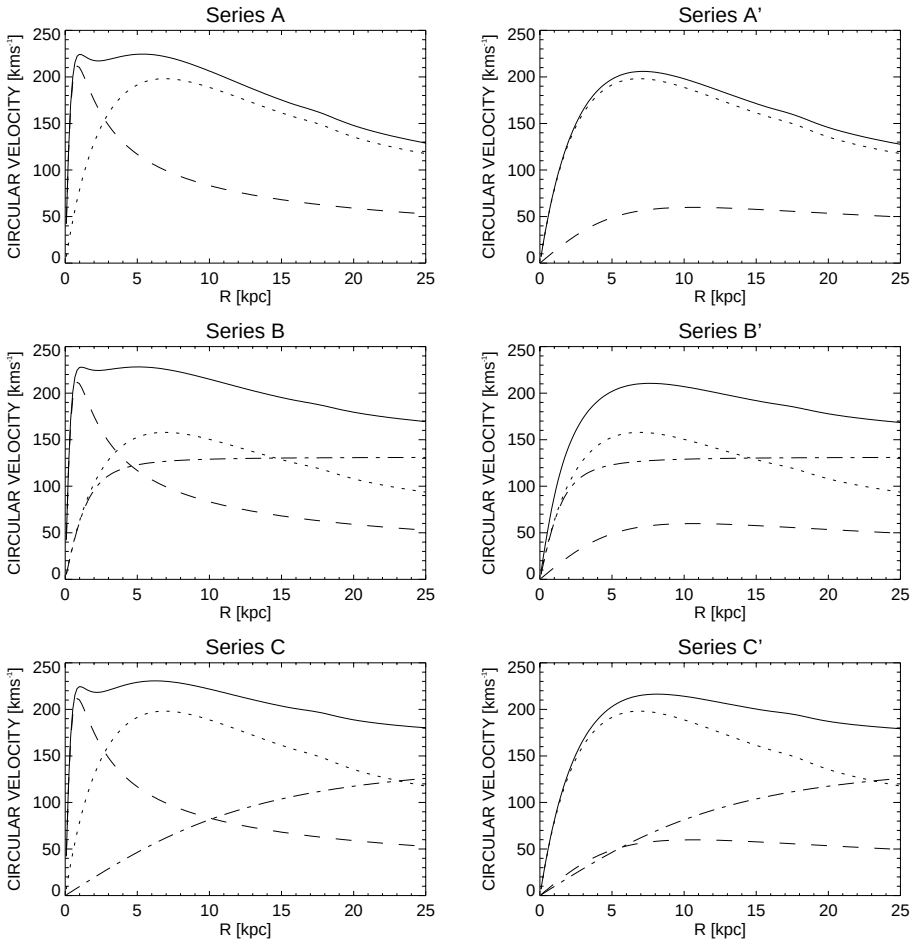

Fig. 1. The initial rotation curves of the mass models used. The continuous line shows the rotation curves. Contributions of the disk (dotted line), the bulge (dashed line) and the halo (dash-dotted line) are also shown.

the corotation resonance (CR) of the bar mode is roughly at the same distance as the inner Lindblad resonance (ILR) of the spiral mode. This is exactly the coupling suggested by Tagger et al. (1987) and the same as was present in the simulation by Masset & Tagger (1997). The gas morphology at this stage is a two-armed spiral, which occasionally forms short-lived pseudorings of both subclasses. A more robust outer pseudoring of subclass R_2' forms by $T = 3$ Gyr and evolves into a complete detached outer ring in a few gigayears. The amplitude spectra of the gas component shows that both of the previously discussed modes affect the ring, although the contribution of the bar mode increases with time. This is not surprising since at $T = 10.0$ Gyr the slower modes have weakened below the lowest contour level of Fig. 3. The major axis of this ring changes from about 20 kpc to about 23 kpc during the simulation, following the change in the bar pattern speed. The axial ratio is about 0.9. Thus the whole ring is considerably beyond the outer Lindblad resonance (OLR) radius, 14–17 kpc, calculated from the epicycle approximation. The closest resonance to the ring is the inner 4/1 resonance of the slower spiral mode. This model develops neither inner nor nuclear rings.

The next model with a higher value of the Toomre parameter, A1.75, evolves more slowly than model A1.25: the formation of the bar takes place by $T = 1$ Gyr. However, the bar is preceded by an oval (here we define the oval – bar boundary to be at a major to minor axis ratio $a/b = 2$), which has formed by $T = 0.4$ Gyr. The outer slowly-rotating spiral mode is much weaker than in model A1.25, but there is a nuclear bar (forms by $T = 0.7$ Gyr) that rotates with a higher pattern speed than the main bar. Note that this nuclear bar forms without the presence of a massive dissipative component, which is not in accordance with the results of Friedli & Martinet (1993). The nuclear bar is associated with a spectacular elongated nuclear ring (forms by $T = 1.2$ Gyr): the position angle of the ring with respect to the main bar changes constantly. The major axis of the nuclear ring changes from 1.6 kpc to 0.75 kpc during the simulation. At the same time, the axial ratio changes from 0.73 to 0.5. This model has only a transient inner ring appearing just after the formation of the bar. The outer pseudoring (subclass R_2') forms soon after bar formation, and is very close to the outer Lindblad resonance of the bar. During next few gigayears it becomes larger and reaches the stage of a detached ring, although the stellar spiral occasionally restores the connection to the central bar.

In model A2.25 a large scale bar does not appear until $T = 9$ Gyr. However, there is a large-scale oval that forms by $T = 3.5$ Gyr. A nuclear ring and weak inner and outer pseudorings emerge in the gas component during the era of the oval. Although there is also a rapidly rotating nuclear bar present, the nuclear ring is related to the oval, being just inside the outer of its inner Lindblad resonances. Rather round inner and outer

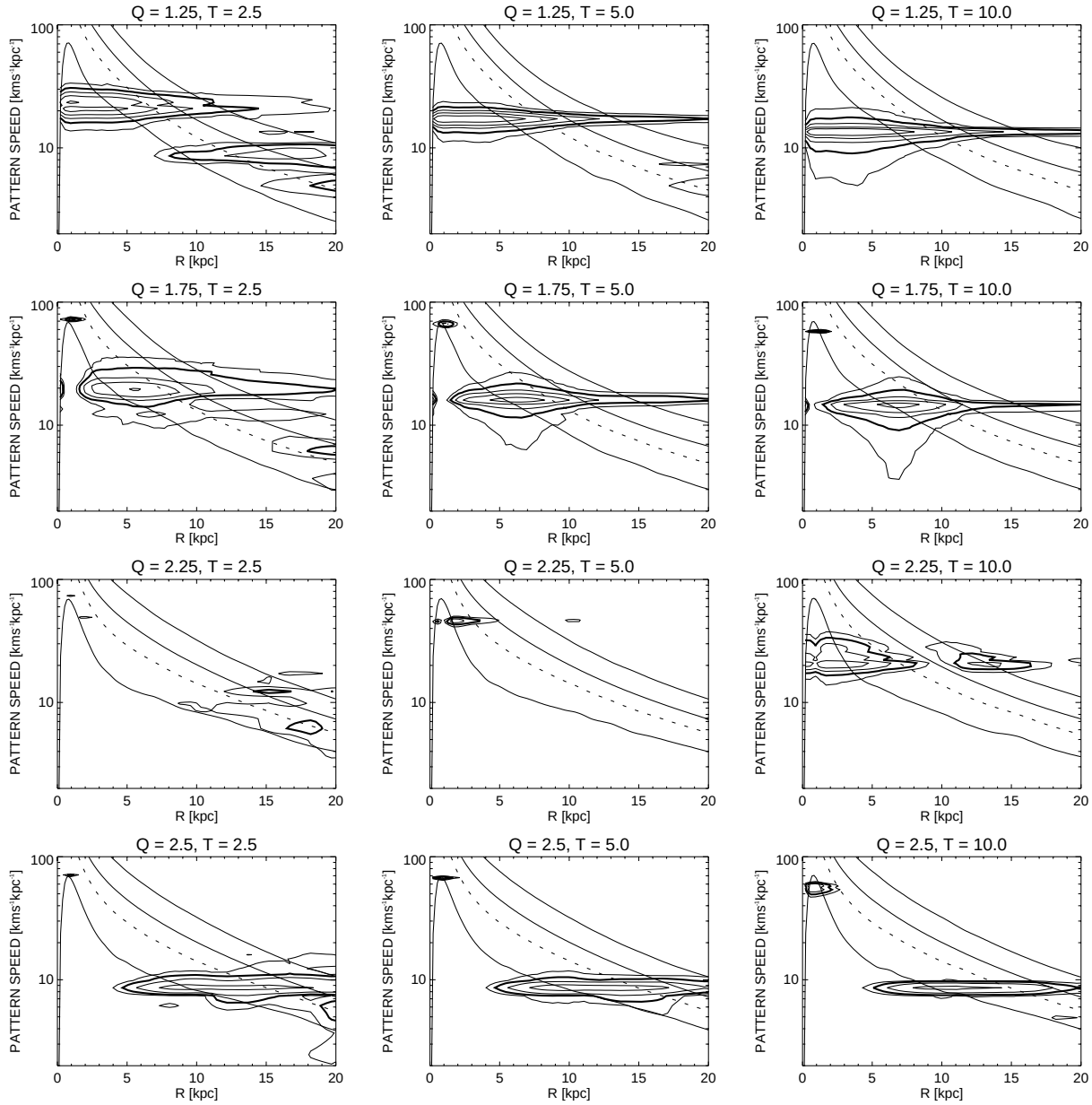

Fig. 2. The $m = 2$ amplitude spectra of the stellar component for family A models, differing in initial value of $Q_{\rm T}$. The contour levels are 0.025, 0.05 (drawn with a thicker line), 0.1, 0.2 and 0.4. The curves showing $\Omega_{\rm c}$ and $\Omega_{\rm c} \pm \kappa/2$ are plotted with a continuous line and $\Omega_{\rm c} - \kappa/4$ with a dotted line. The length of the used time interval is 2.5 Gyr. The middle points of the time intervals are indicated in gigayears in the top of each frame. Note that the vertical axis has a logarithmic scale.

pseudorings are close to the corotation and OLR of this mode, respectively. When the bar forms (see Fig. 2), its pattern speed is lower than that of the previously discussed oval, and considerable rearrangement of the gas morphology takes place. An inner ring forms in about 700 million years between the inner 4/1- and the corotation resonances of the bar, and an outer pseudoring forms about 400 million years later, very near the OLR. The spiral arms composing this pseudoring start outside the inner ring. The isodensity curves of the stellar component become almost circular near the inner 4/1-resonance, giving the impression that the bar does not fill the major axis of the inner ring completely. The evolution of the nuclear ring is very curious after the bar forms: the nuclear ring is captured by the nuclear bar and becomes smaller (from 1.3 kpc to 0.7 kpc) and less elongated (from 0.67 to 0.78).

The model with the highest Toomre parameter, A2.5, does not develop a clear bar but rather an oval that forms by $T = 1.5$ Gyr. Because the pattern speed of the oval is rather slow, so that its OLR is much farther in the outer disk than in the previous models, we found it necessary to use a wider gas distribution with 40 000 particles. The oval is surrounded by an inner ring, which forms by $T = 2$ Gyr. This model also has a nuclear bar and a huge nuclear ring (radius 6.4 kpc), which forms at the same time as the inner ring and is also related to the oval. In

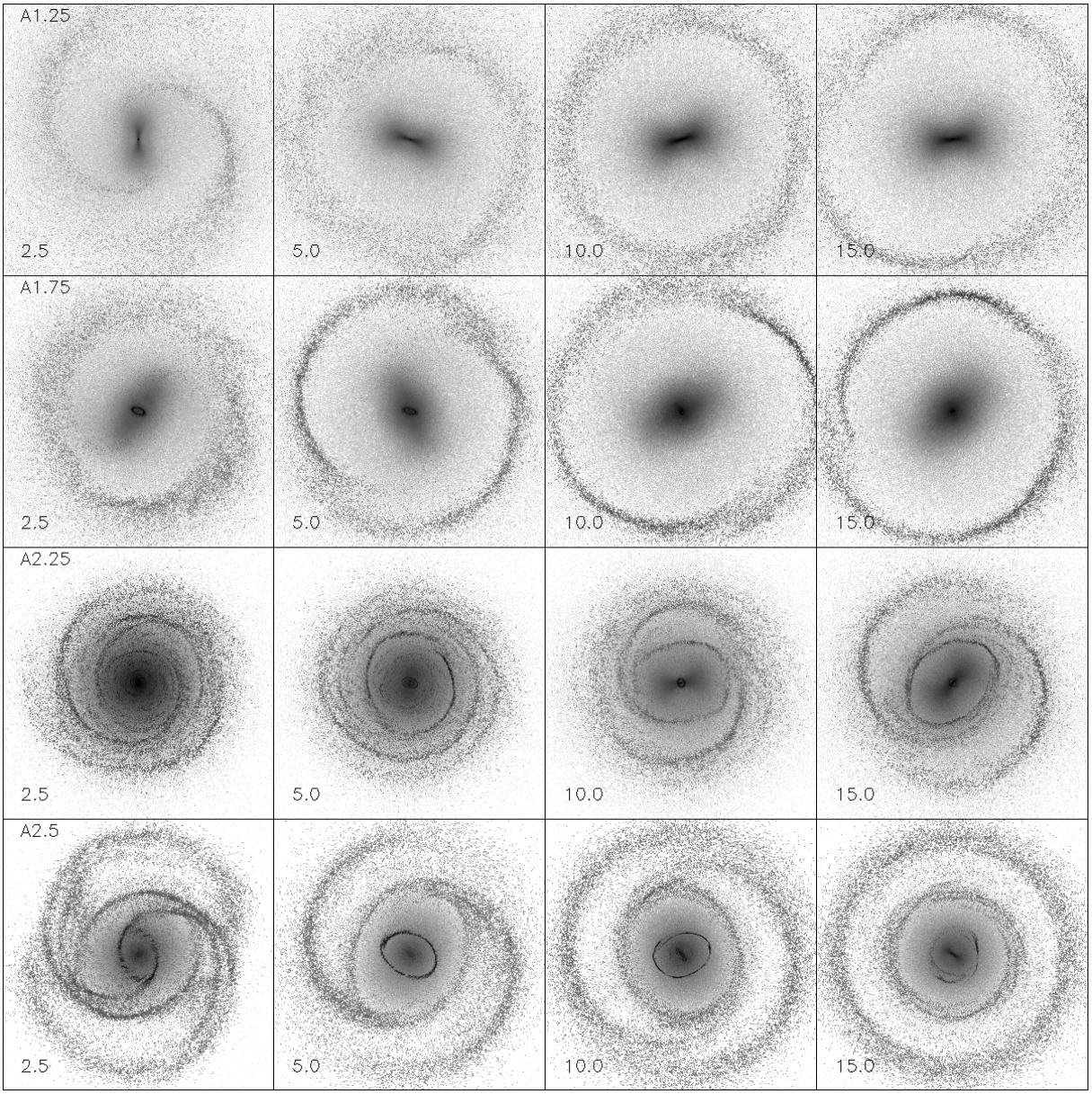

Fig. 3. The evolution of the family A models with $Q_{\rm T} = 1.25$, 1.75, 2.25 and 2.5, from the uppermost to the lowermost row, respectively. The morphology is shown at T = 2.5, 5.0, 10.0 and 15.0 gigayears from the beginning of the simulation. The gas density is multiplied by 20 to show it more clearly. The width of the frames is 45 kpc, except for model A2.5 where it is 60 kpc.

the early stages of the simulation, features resembling leading offset dustlanes connect the nuclear and the inner rings. The outer pseudoring, which forms by $T = 2.6$ Gyr, evolves from subclass R_1' to R_2'. Later, when the oval practically disappears, the rings become almost circular, and the system resembles the galaxy NGC 7217, studied by Buta et al. (1995a) and Verdes-Montenegro et al. (1995). It is remarkable that the oval dissolves, even though the often mentioned processes leading to bar destruction (namely massive gas inflow (see e.g. Friedli & Benz. 1993) or an encounter with another galaxy (e.g. Athanassoula 1996)) are not present. In this model, the cause of the disappearance of the oval is probably the strengthening of the nuclear bar. All the major rings in this model have the same pattern speed as the oval.

3.2. Models with a strong halo

Models with a strong halo (the amplitude spectra are shown in Fig. 4 and the morphological evolution in Fig. 5) do not form a bar as quickly as the disk dominated models. The early phases in the evolution of these systems typically show multiarmed or even flocculent spiral structures. Another difference compared to disk dominated systems is that the importance of the bar mode is smaller: the slower modes are usually strong, or even dominating, near the outer Lindblad resonance of the bar. The

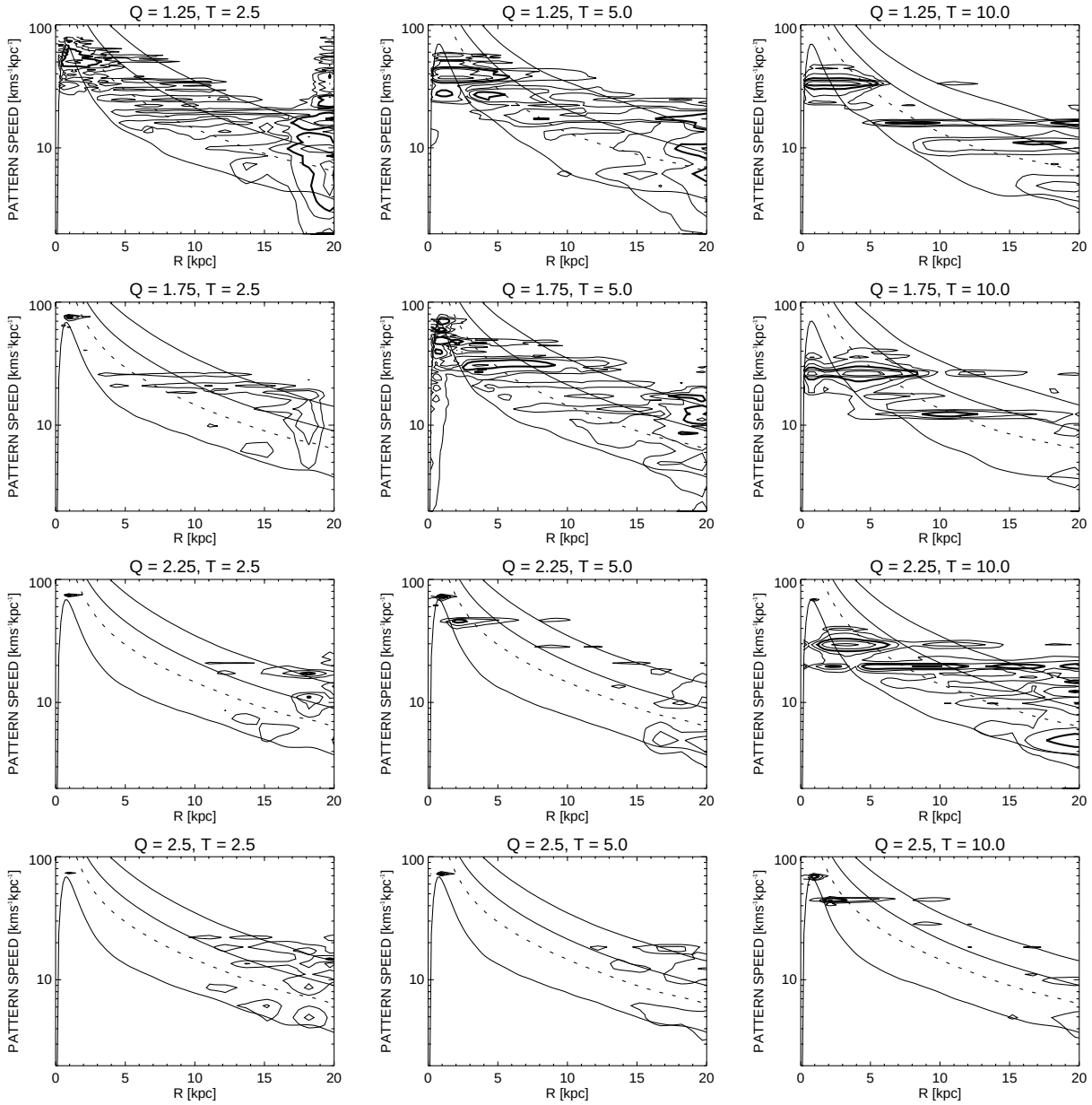

Fig. 4. The $m = 2$ amplitude spectra of the stellar component for the model family B.

dominance can start from the corotation radius of the bar, as in model B1.25.

The first six gigayears of model B1.25 are characterised by a multiarmed spiral structure (three- and four-armed spirals are also present in the stellar component), even after the bar formation at $T = 2.5$ Gyr. The small bar component is surrounded by a rather round inner pseudoring that forms about 200 million years later. When the bar strength increases, the pseudoring becomes a more elongated (reaching an axial ratio of 0.73 by $T = 10$ Gyr) continuous ring. By $T = 7.5$ Gyr, the outer disk forms a detached outer ring, which seems to consist of two nested structures. The inner ring is very close to the inner 4/1 resonance of the bar, but the outer ring is not at any specific resonance of the two slower modes, which have peaks in the amplitude spectrum of the gas near the ring radius. For several gigayears, this model has a four-mode-chain of CR – inner 4/1 resonance overlappings, resembling several models in Rautiainen & Salo (1999).

Model B1.75 forms a large scale bar more slowly than model B1.25, by $T = 5.5$ Gyr, although there is an oval for about one gigayear before that. However, there is a nuclear bar that forms by $T = 1$ Gyr, and is captured by the main bar by $T = 6.3$ Gyr. A short-lived nuclear ring forms by $T = 5$ Gyr: it disappears about the same time as the large scale bar forms. By $T = 6.3$ Gyr, the multiarmed structure disappears as the model develops an outer pseudoring and a weak inner ring (not clearly visible in Fig. 4). At the early stage, the morphology of the outer pseudoring is somewhere between subclasses R'_2 and $R_1R'_2$, but

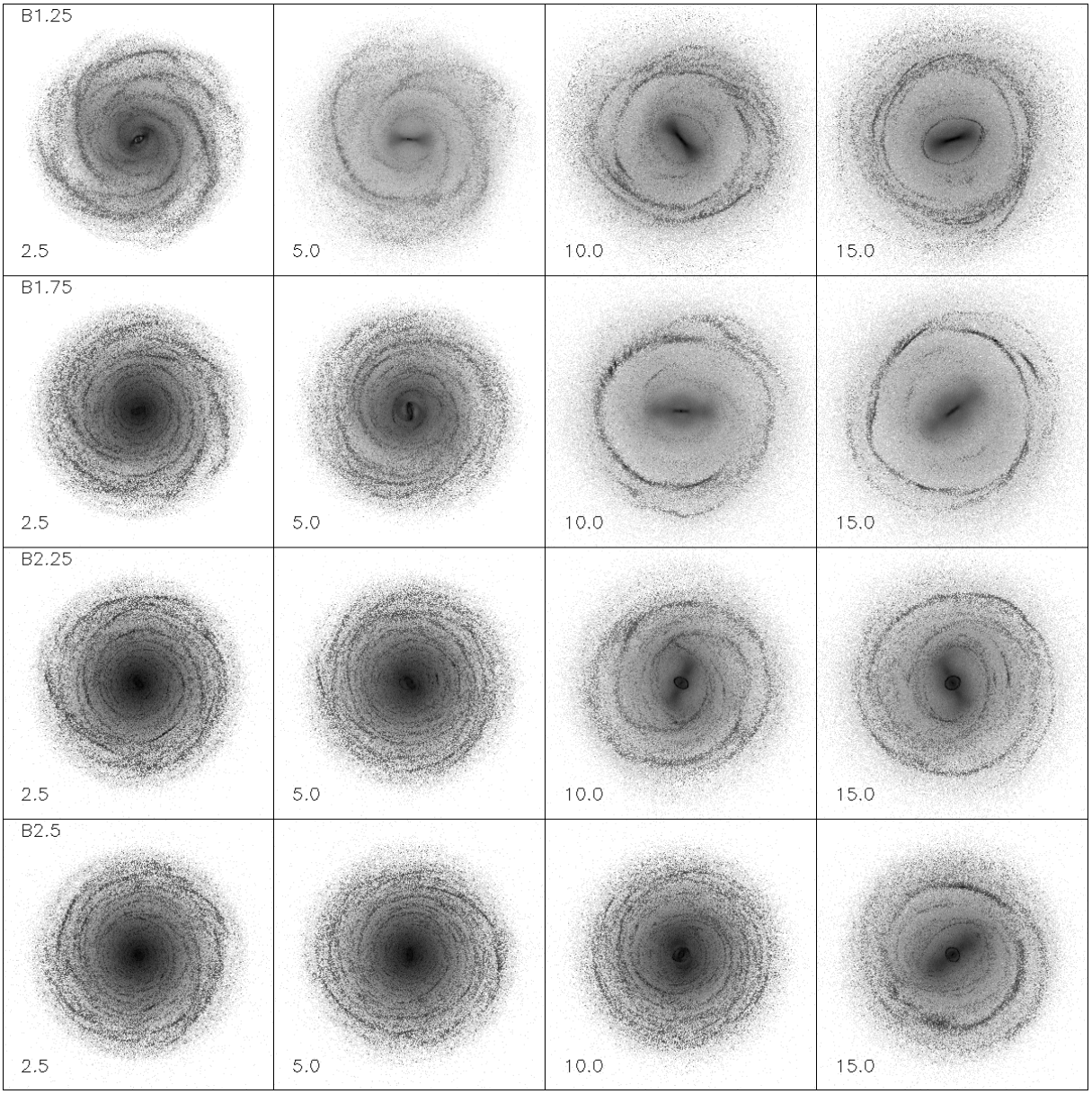

Fig. 5. The evolution of the family B models with $Q_{\rm T} = 1.25$, 1.75, 2.25 and 2.5. The morphology is shown at the same timesteps as for family A.

later the ring becomes detached from the bar. Occasionally the evolving stellar spiral has clear R_1' morphology, even when the gas component lacks it. The inner ring is completely inside the corotation resonance and very close to the inner 4/1-resonance. The strongest peak in the amplitude spectrum of the gas in the outer ring is related to a slower mode, although the bar mode also gives a strong signal. The outer ring, with a radius of about 14 kpc, is almost exactly midway between the OLR of the bar and the corotation of the slower mode, 12.5 and 15.5 kpc, respectively.

In model B2.25 the evolution is again slower than in the previous model; an oval forms by $T = 5.1$ Gyr and becomes a bar about 500 million years later. The bar formation coincides with the formation of a nuclear ring near the inner Lindblad resonance of the bar. Although there is a fast rotating nuclear bar from $T = 1.2$ Gyr, a nuclear ring forms by $T = 5.1$ Gyr and the amplitude spectrum clearly shows that the ring follows the main bar/oval. The inner ring is a totally different story: it follows mostly an outer oval (forms by $T \approx 8$ Gyr) with a slower pattern speed than the bar, which makes the ring often misaligned with the bar. A more detailed discussion of this is given in Sect. 4.3. The outer structure of this model has a changing morphology, evidently due to the effect of several modes.

Model B2.5 develops an oval at $T = 9.5$ Gyr, but the formation of a clear bar does not take place until $T = 13$ Gyr. Although there is a nuclear bar from $T = 2.8$ Gyr, a nuclear ring forms by $T = 9.5$ Gyr, and is close to the ILR of the oval with a pattern speed $\Omega_{\rm p} = 45$ kms^{-1}kpc^{-1}. Another nuclear ring develops temporarily inside this ring, but it is related to a faster mode. At $T = 12.5$ Gyr there is also an outer pseudoring.

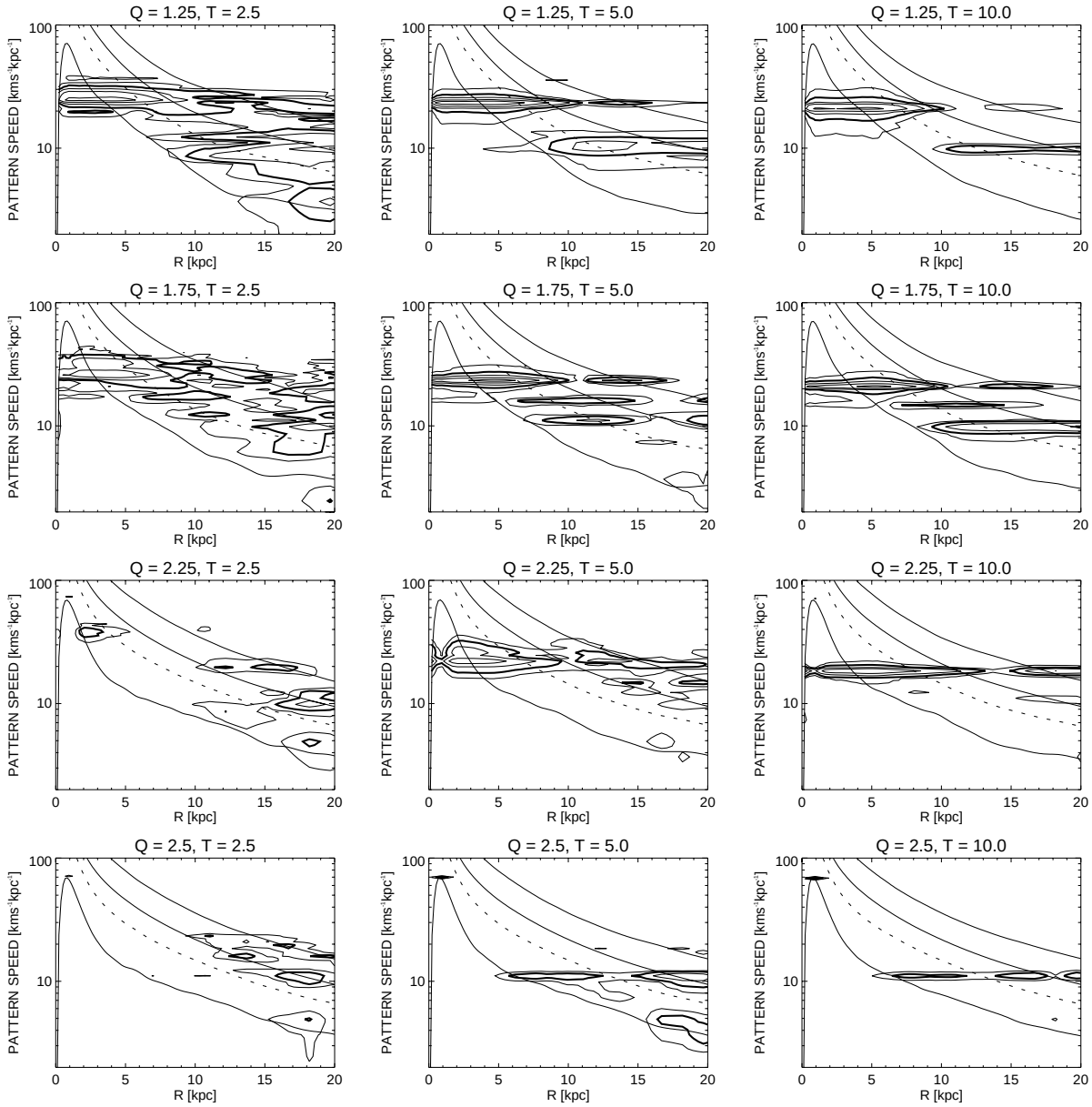

Fig. 6. The $m = 2$ amplitude spectra of the stellar component for the model family C.

When the bar finally forms (with $\Omega_{\rm b} = 29.4$ kms^{-1}kpc^{-1}), it develops an inner ring between its inner 4/1- and corotation resonances. It also captures or adopts the nuclear ring formed by the now-disappeared $\Omega_{\rm p} = 45$ kms^{-1}kpc^{-1} mode: although the ring is located well inside the ILR radius calculated from the epicycle approximation and although there is a nuclear mode present, the nuclear ring follows the main bar after $T = 13.75$ Gyr. The outer pseudoring with an evolving structure is close to the OLR of the bar, but shows also the effect of a slower mode in its amplitude spectrum.

3.3. Models with a moderate halo component

Debattista & Sellwood (1998) demonstrated that systems in which the halo dominated inside the region of the optical disk (as is the case in our model family B) are not necessarily very realistic models for barred galaxies. Namely, when a massive self-consistent halo component was included in their 3D-models, the pattern speed of the bar decreased so much that the bar ended well before the corotation resonance, which disagrees with most of the modelling results for individual observed galaxies (e.g. Hunter et al. 1988; Lindblad et al. 1996). For this reason, we also made simulations with a model where the halo component is moderate and its contribution to the rotation curve rises above the disk contribution only in the outermost part of the disk. Fig. 6 shows the amplitude spectra and Fig. 7 the morphological evolution of these models.

The model with the coolest disk, C1.25, develops a bar at $T = 0.5$ Gyr. An outer ring structure forms about 1 Gyr later. This evolves from a pseudoring very close to the OLR of the bar

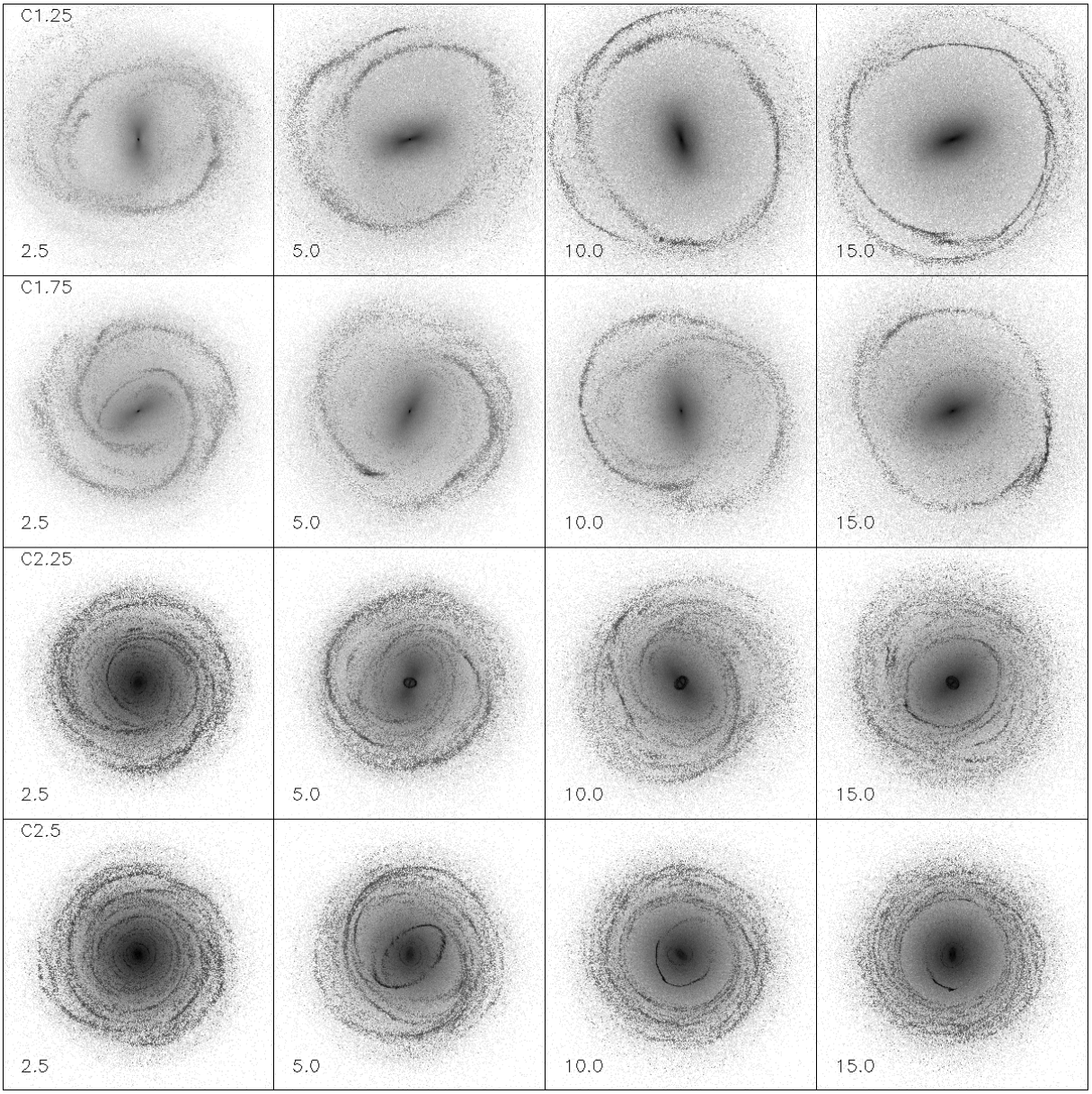

Fig. 7. The evolution of the family C models with $Q_{\rm T} = 1.25$, 1.75, 2.25 and 2.5. The morphology is shown in the same timesteps as for family A.

to a detached outer ring outside the OLR radius. The morphology of the ring keeps changing throughout the simulation and a subclass cannot usually be determined. Occasionally there is a combined outer ring of subclass R_1R_2', where the R_1 component is present practically only in the stellar component, whereas the R_2' part dominates the gas component. Although the ring is rather close to the OLR of the bar, the strongest peak in the $m = 2$ amplitude spectrum of the gas in the ring area is related to a mode with lower pattern speed. There are no inner or nuclear rings in this model.

Changing outer ring morphology is also typical for model C1.75, where the outer pseudoring forms very quickly, only about 200 hundred million years after the bar formation, at $T = 1.3$ Gyr. The outer pseudoring can often be classified as either R_2' or R_1R_2' (where the R_1 component can be enhanced by the stellar component), but sometimes we found detailed classification impossible: we could only say that it was a pseudoring (R'). A more detailed coverage of the early evolution of the gas component in this system is shown in Fig. 10. The time scale of considerable changes in the outer ring morphology can be as short as 100 million years, when the typical orbital period near the ring radius is about 500 million years. The amplitude spectrum of the gas component shows that the outer ring is affected by both the bar mode and the mode with a slower pattern speed, the latter being the dominating one. The ring is located between the OLR of the bar and the corotation of this slower mode. An inner ring or a pseudoring forms at about the same time as the outer pseudoring and it is located between the inner

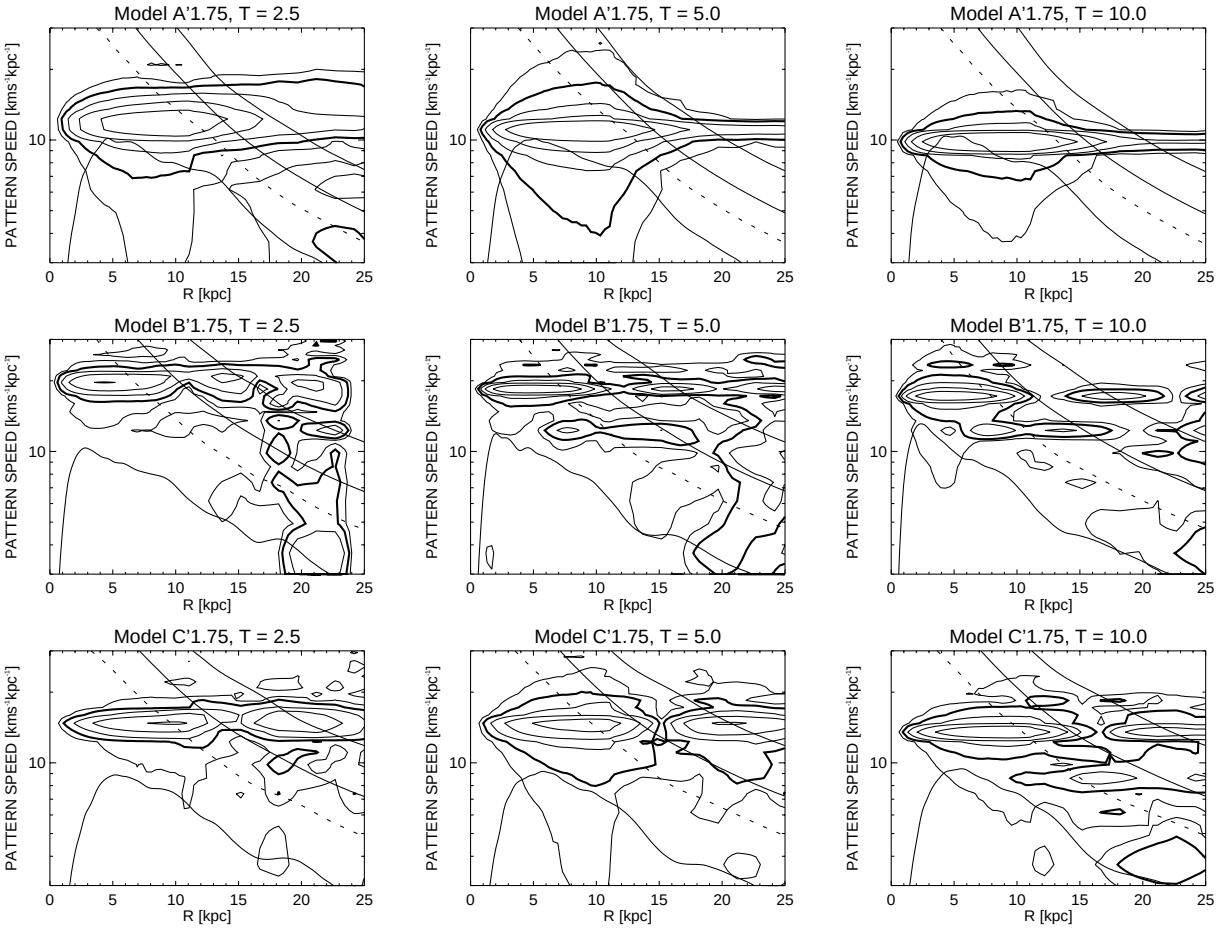

Fig. 8. The amplitude spectra of the stellar component for models A'1.75, B'1.75 and C'1.75, which have slowly rising rotation curves.

4/1-resonance and the corotation of the bar. This model also has a shrinking nuclear ring that is destroyed in few hundred million years. A better resolution plot of the evolution of this and a few other nuclear rings is shown in Fig. 13.

Model C2.25 develops an oval and a nuclear bar by $T = 0.9$ Gyr and a large scale bar by $T = 3$ Gyr. There are short-lived inner and outer pseudorings during the oval stage, but a more robust outer structure forms by $T = 3.9$ Gyr. This evolves continuously, and cannot usually be classified into outer ring subclasses. In later phases of the simulation, the outer morphology becomes almost flocculent. On the other hand, there are very steady inner and nuclear rings in this model. The inner ring forms by $T = 3.4$ Gyr and is located between the inner 4/1- and corotation resonances of the bar, being closer to the former one of the resonances. At $T = 15$ Gyr, the bar does not fill the major axis of the inner ring completely, thus resembling model A2.25. Although there is a nuclear mode inside the nuclear ring, the amplitude spectrum shows that the ring follows the main bar. The nuclear ring forms by $T = 2.1$ Gyr, initially exactly to the (outer) ILR of the oval, at a radius of 1.7 kpc. Then the ring shrinks so that its major axis is about 1.4 kpc, while the ILR moves outwards to radius of 2.3 kpc, following the deceleration of the bar rotation.

The model with the hottest disk, $Q_{\rm T} = 2.5$, lacks the main bar component, but it still has ring structures. Although there is a nuclear bar present, the most spectacular ring is related to the spiral component (see Fig. 16, and discussion in Sect. 4.3), being near its ILR. The outer disk has a flocculent gas morphology and is separated by a gap from the inner region.

3.4. Models with slowly rising rotation curves

We also made simulations where we modified the bulge model so that the rotation curves rise more slowly. Fig. 8 shows the amplitude spectra of three such simulations, all with $Q_{\rm T} = 1.75$, and Fig. 9 presents the corresponding evolution. In all these models, the bar is longer than in the corresponding model with a steeper rotation curve. Excluding the last stages of Model A'1.75, these models do not have an inner Lindblad resonance, and thus it is not surprising that they do not develop nuclear rings. They also lack nuclear bars.

In model A'1.75, we found it necessary to widen the initial gas distribution to be able to cover the OLR region. When doing so, we also increased the gas particle number to 40 000. This model develops an oval by $T = 0.6$ Gyr, and a bar about 200 million years later. A detached outer ring, whose radius (about 30 kpc) is about twice the bar major axis, but it is not related

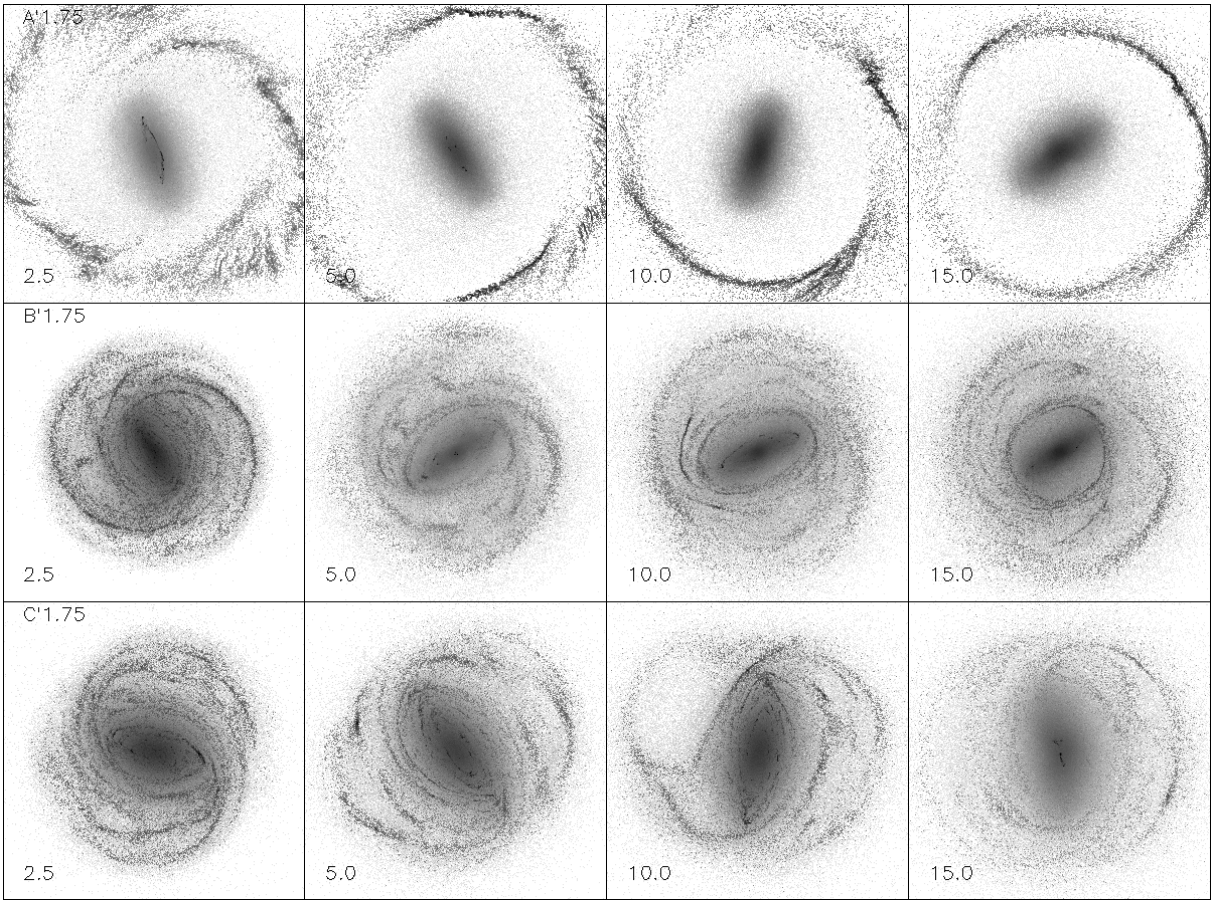

Fig. 9. The evolution of model A'1.75, B'1.75 and C'1.75. In model A'1.75, the width of the frame is 66 kpc, in others it is 45 kpc.

to any resonance induced by the bar: the OLR of the bar is at 20 kpc. What makes this ring even more strange is that the amplitude spectrum of the gas component has peaks at pattern speeds which do not correspond to any clear modes in the stellar component.

Model B'1.75 develops a bar by $T = 1.6$ Gyr, and it has an inner ring (from $T = 2.5$ Gyr) that is first very elongated, but becomes more circular towards the end of the simulation. For several gigayears, there is an additional elongated ring component just inside the main part of the inner ring. The inner ring is very close to the inner 4/1-resonance. The outer morphology changes, but can be occasionally classified using the outer ring subclasses. Both the corotation of a slower mode and the outer Lindblad resonance of the bar are close to the ring radius. According to the amplitude spectra, the bar mode dominates in the ring radius.

Model C'1.75 develops first an oval ($T = 1$ Gyr) and then a bar ($T = 1.9$ Gyr). There is a rather similar two-component inner ring (since $T = 1.2$ Gyr) as in model B'1.75, but now the inner, very elongated component is more pronounced. The major axis of the more elongated component is close to the inner 4/1-resonance of the bar, whereas the outer component is between the inner 4/1- and corotation resonances. This model also has an outer pseudoring (from $T = 2.3$ Gyr), which is of subclass R'_1, although its shape is often quite unusual: at early stages there is a secondary pair of spiral arms and later the ring is lopsided. The major axis of the outer pseudoring is close to the outer 4/1-resonance of the bar, which is a rare situation in our simulations. Both the inner and the outer rings follow the bar mode.

4. Discussion

In this section we discuss, based on our simulations, the different aspects related to the formation and the evolution of rings, both in barred and non-barred galaxies. Finally, we discuss the limitations of our modelling approach.

4.1. The relationship of bars, rings and resonances

We determined the major and minor axes of the rings in selected timesteps (3–4 per simulation) in our 15 models. From these we have calculated the ratios of the geometrical mean radii of outer pseudorings of subclasses R'_1 and R'_2 to the OLR radii of the bar. For R'_1 pseudorings the average ratio is 0.892 and for R'_2 pseudorings it is 1.143. This clearly shows that the outer rings tend to be located near the outer Lindblad resonance of the bar, the first subclass inside and the second subclass outside the OLR radius. The simulations applying a rigid bar potential in modelling the behaviour of the gas component (Schwarz 1981;

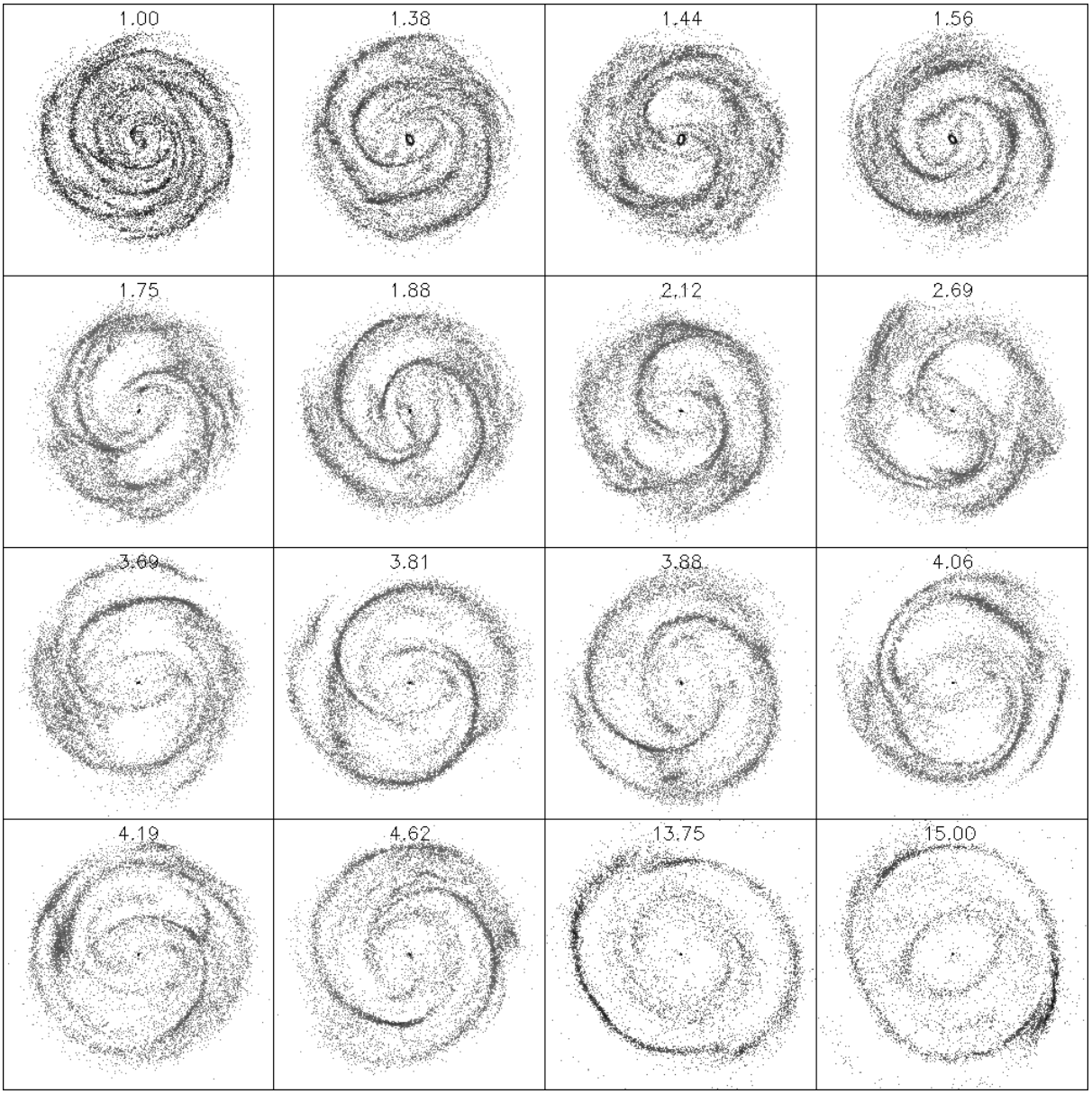

Fig. 10. The outer ring evolution of the model C1.75. Only the gas component is shown. Time is shown in gigayears. The outer ring morphology is evolving constantly, e.g. R'_2: T = 1.56, 1.88, 3.88; $R_1R'_2$: T = 1.44, 2.69, 4.19.

Byrd et al. 1994) suggest that the two different subclasses of outer rings can be explained by two major orbit families in the vicinity of the OLR. Which one is occupied depends either on evolutionary stage or on gas distribution. However, N-body simulations provide other possibilities. For example, there can also be a spiral mode in the outer disk with a lower pattern speed than the bar. In such cases the morphology of the outer ring is not steady: it keeps changing between different outer ring subclasses and occasionally the morphology does not resemble either of them (see Fig. 10).

This cyclic behaviour suggests that there may not always be a profound difference between galaxies of different outer ring subclasses. This would mean that the evolutionary change from subclass R'_1 to R'_2, as suggested by Byrd et al. (1994), is not the reason for the existence of two ring subclasses. The cyclic change also disagrees with Buta & Crocker (1991), who found a correlation between the outer and the inner structures. According to their results, galaxies with outer ring subclasses R'_1 and R_1 tend to have inner and nuclear rings and dust lanes, whereas galaxies of subclass R'_2 usually lack them. Buta and Crocker's original analysis was based on only 22 galaxies but they later enlarged the sample (Crocker & Buta 1993). One should also note that the observed correlation was not exclusive: there are galaxies of subclass R'_2 with nuclear rings and those of subclass R'_1 without them.

Many outer ring structures in our simulations could not be comfortably classified to subclasses. Pseudorings could have mixed characteristics: either the orientation of the major axis

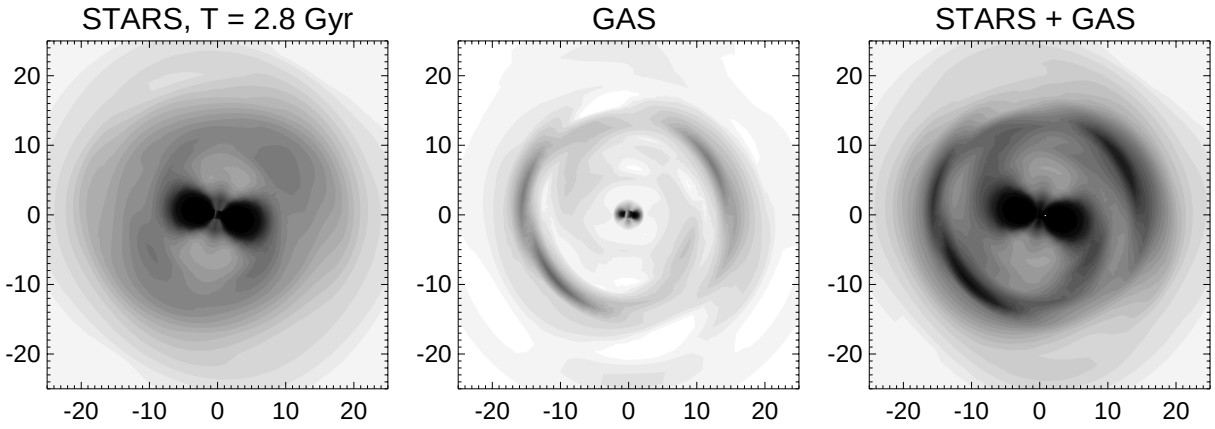

Fig. 11. The double outer ring of model C1.25 as seen in stellar, gas and combined distribution. Reconstructed from Fourier decompositions using $m = 0$,1,2,3 and 4 components.

or the winding of the spiral arms was between the values typical for subclasses R_1' and R_2' or the arms where asymmetric, one arm behaving like R_1' pseudoring and the other like R_2'. Such problems exist also with real galaxies: for example, the outer pseudoring of NGC 1300 is elongated about 70° to the bar (Elmegreen et al. 1996). In addition to previous difficulties, it was usually impossible to give a subclass for complete detached outer rings, which formed from pseudorings after the evolution of several gigayears.

Another element of outer ring classifications is provided by different morphologies of the stellar and gas components. Although ring formation usually takes place only in the gas component, there are a few cases in our simulations where the stellar spiral arms also form an outer pseudoring. Stellar pseudorings are much broader than gaseous rings, and usually are not steady because they form and dissolve repeatedly. In a few cases, like model C1.25 in Fig. 11, there is a R_1R_2' morphology, where the gas component forms the R_2' part, whereas the stellar component enhances or solely forms the R_1 part. Interestingly, there are some observed cases where the situation can be rather similar: NGC 6782, which has a partial R_2' pseudoring in H_α, whereas the continuum image has R_1 morphology (Crocker et al. 1996) and IC 1438, which has strong R_2' morphology in a B-band image, but a R_1 morphology in I-band (Byrd et al. 1994; Buta 1995). Byrd et al. (1994) suggested that in IC 1438 the R_1 component formed first in the gas component and left a remnant in the stellar component after evolving to R_2' stage. However, based on our new simulations, we think that at least some stellar R_1 rings are not remnants, but phenomena of self-gravitating stellar component.

The inner rings have traditionally been thought to be related to the inner 4/1-resonance of the bar. Indeed, in low amplitude simulations with a rigidly rotating bar potential, they appear as four extremely tightly wound spiral arms precisely in this resonance (see e.g. Fig. 7 in Salo et al. 1999), which firmly supports the hypothesis. When the amplitude is increased, their shape evolves to a complete ring. At the same time, the ring major axis moves towards the corotation resonance and the ring becomes more elongated. The N-body simulations agree well with this picture. The average ratio of the geometrical mean radius of inner rings to inner 4/1-resonance radius was 1.0, whereas the corresponding ratio to the corotation radius was 0.72. The inner ring major axis is often between the previously mentioned resonances, usually closer to the inner 4/1. Few inner rings are completely inside the inner 4/1-resonance. Sometimes, e.g. models A2.25 and C2.25, the density plots give an impression that the bar ends before reaching the inner ring. There are also real galaxies showing the same phenomenon: the bar fills the inner ring major axis incompletely. An example of this is NGC 7098, where this can be seen in the B-band CCD-image (see Fig. 35 in Buta 1995) and also in the second generation red image of the STScI Digitized Sky Survey.

The nuclear rings are usually thought to be related to the inner Lindblad resonance of the main bar or alternatively to a nuclear bar component. Both situations are present in our simulations. When related to the main bar component, the nuclear ring is usually not in either of the ILR radii, but between them. Here one should note that the resonance radius calculated from the epicyclic approximation is not reliable in the case of strong perturbations: the stronger the bar, the smaller are the nuclear rings (see e.g. Fig. 7 in Salo et al. 1999). When the bar is very strong, the x_2 orbits (see Contopoulos & Grosbøl 1989) supporting the nuclear rings can become unstable.

Although there are simulations where the nuclear ring clearly follows a nuclear mode with a higher pattern speed than that of the main bar (e.g. model A1.75), the presence of a nuclear mode does not necessarily mean that the nuclear ring follows it. There are also cases where a nuclear bar precedes the main bar by several gigayears (e.g. model C1.75), but a clear nuclear ring does not form until a main bar is pesent. Apparently, the nuclear bar alone is usually insufficient to transport gas to the central area to form a ring. In a few of our models there are two nuclear rings: the outer one following the main bar and the inner one following the nuclear mode. It is not clear if this is the case with the few observed galaxies with double nuclear rings (e.g. NGC 1317; detected in H_α by Crocker et al. 1996 or M83; detected in near-IR by Elmegreen et al. 1998), the other possibility is that the rings are related to the two inner Lindblad resonances of the

Table 1. The axial ratios of the different ring types in the simulations, compared with the observed sample.

Ring type	Simulations	Buta 1995
R'_1	0.80	0.74 ± 0.08
R'_2	0.91	0.87 ± 0.06
r, rs	0.77	0.81 ± 0.06
nr	0.70	

Table 2. Average relative diameters of rings in simulations and observations (Buta & Crocker 1993). For simulations both the ratio of major axes, β, and the ratio of geometrical mean diameters, ρ, were determined.

Ratio	β	ρ	BC93
R/r	2.0	2.2	2.2
R/nr	12.0	14.4	18.9
r/nr	5.2	5.3	8.7

main bar. Another interesting phenomenon is the capture of nuclear rings, which happens in some of our simulations: when a mode originally forming the ring fades, another mode can adopt the ring, and possibly change its radius.

The average minor to major axis ratio is 0.80 for R'_1 pseudorings and 0.91 for R'_2 pseudorings (see Table 1). This means that outer pseudorings of both subclasses are a bit more circular than in the observations by Buta (1995), where the corresponding ratios were 0.74 and 0.87. The average minor to major axis ratio of the inner rings and pseudorings is 0.77, whereas in the Catalogue of Southern Ringed Galaxies it is 0.81. The average minor to major axis ratio of the nuclear rings in our simulations is 0.70, the extreme values being 0.39 and 1.0. Unfortunately, precise statistics about the intrinsic shapes of the observed nuclear rings are not available to be compared with our simulation data (Buta & Combes 1996), but a rough estimate of the average axis ratio is about 0.9, varying from 0.6 to 1.0 (Crocker & Buta 1993; Buta, private communication).

We have also determined the relative sizes of rings. Table 2 shows both the major axis ratios β and the ratios of geometrical mean radii ρ and compares them with the observations. The average ratio of geometrical mean radii of outer and inner rings is 2.2, very close to what is observed (Buta & Crocker 1993; Buta 1995). However, this accuracy is partly coincidental, the corresponding ratios for model families A, B and C are 1.9, 2.6 and 1.9, respectively. Our selection of models, which shows a wide variety of different morphologies, was composed to study the effect of different mass models and values of $Q_{\rm T}$. Thus, it probably does not correspond to any realistic galaxy sample. This is more clearly seen when comparing the relative sizes of the nuclear rings with the observations. For average values of ratios $\rho(R/nr)$ and $\rho(r/nr)$ we obtained 14.4 and 5.3, respectively, whereas the observed values are 18.9 and 8.7. Thus, the nuclear rings in our simulations are larger than the observed ones. Part of this discrepancy is caused by few anomalous cases in our selection of models, especially the huge nuclear ring of model A2.5. Omitting such cases would make our results closer to the observed values. Another possible factor is the uncomfortably large value of the softening parameter ϵ when compared to the sizes of most of the nuclear rings in our simulations. A considerably smaller value of ϵ would correspond to an unrealistically thin disk and thus we leave further studies of this problem to forthcoming three-dimensional simulations.

4.2. The absence of rings in barred galaxies

The absence of rings in many barred galaxies also requires an explanation. In the case of outer rings, there are several plausible possibilities. If the bar is relatively young, it has had not enough time to form an outer ring, whose typical formation time scale is one gigayear or more (note however that e.g. in model C1.75 an outer pseudoring forms very quickly, about 0.2 Gyr after the bar formation). On the other hand, the formation of a nuclear ring can coincide with bar formation, or occasionally can happen even before a clear bar component has formed, then related to a mode that later becomes the bar. The inner rings can appear quickly, the formation timescales ranging from practically coinciding with formation of the bar to a few hundred million years, although there are also cases where a pronounced inner ring appears only after several gigayears. Interactions with other galaxies can also destroy outer rings (Elmegreen et al. 1992). The third sometimes-mentioned possibility is that the region near the outer Lindblad resonance of the bar is dominated by a slower spiral mode, which inhibits the outer ring formation. However, we found several examples where an outer ring formed in spite of the presence of a slower spiral mode. There were also outer rings where the strongest $m = 2$ amplitude signal came from the slower mode.

The absence of nuclear rings can be related to the strength of the bar: in high amplitude cases the orbits supporting the nuclear ring become unstable. It is also possible that the pattern speed of the bar is sufficiently high, when compared to the peak of the $\Omega_{\rm c} - \kappa/2$ curve, that it does not have an inner Lindblad resonance, and thus cannot form a nuclear ring. This was the case for the three models with slowly rising rotation curves.

Also, the inner rings seem to be absent in simulations with the strongest bars, e.g. models A1.25 and C1.25. However, especially in these simulations, the bar formation is a very violent phenomenon, which includes strong outflow of gas particles. This means that when the bar has settled to a slow evolution, there are not enough gas particles left in the inner regions to form an inner ring in simulation. In real galaxies, the gas component can be refreshed via supernova explosions, stellar winds and gas accretion. To verify if the early outflow is the reason for the absence of inner rings, we also performed simulations where we included the gas component only after the bar had formed and its pattern speed change had decreased. In a few models this can indeed lead to the formation of an inner ring. An example of this is C1.25, shown in Fig. 12. In this particular case, there is also an outer pseudoring of subclass R'_1, which is absent in the original model where the gas was included from the beginning of the simulation (note that this pseudoring is

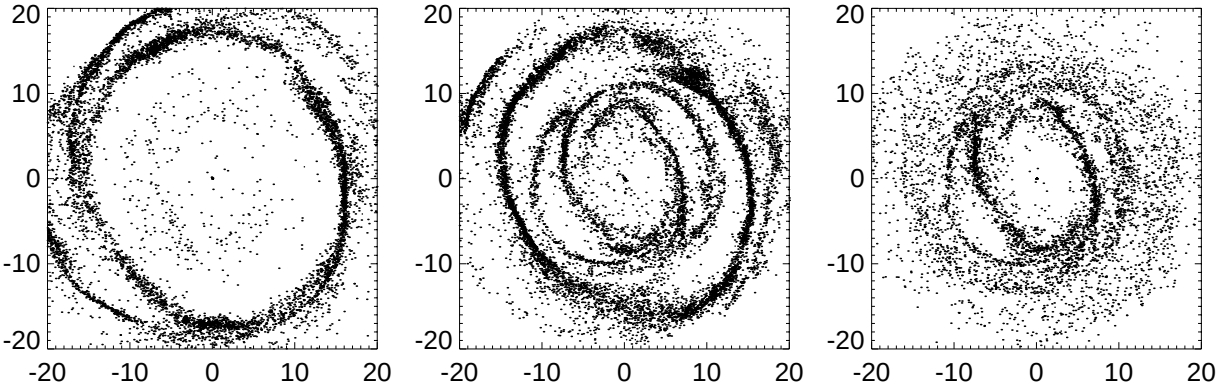

Fig. 12. Comparison of three different gas inclusion methods. The frame on the left shows the gas distribution in a simulation (model C1.25) where the gas particles were included from the beginning of the simulation. The middle frame shows the same model, but the gas particles are included only after bar has formed and its pattern speed change has decreased. The frame on the right shows a model were the gas inclusion was done as in the model shown in the middle frame, but the initial gas particle distribution was exponential.

completely inside outer 4/1-resonance, which is very unusual in these simulations). However, in model A1.25, this procedure did not lead to formation of a clear inner ring.

Inspired by the effect of delayed gas inclusion, we also made a few of our simulations with an exponential initial gas surface density distribution (having the same scale length as the stellar component). When combined with the delayed gas inclusion method for model C1.25, the main effect was the lack of the R_2' component while the R_1' component remained (Fig. 12). This behaviour resembles the simulations by Schwarz (1981), where the outer cut-off radius of the gas component determined which of the pseudoring subclasses was produced. However, such an effect was not clearly present in other simulations, where we included the exponential gas distribution from the beginning. Instead, the outer structures became more diffuse, simply due to reduced number density of particles. In two models, B1.75 and C1.75, long-lasting nuclear rings appeared, possibly due to larger amount of particles in the inner region.

A nuclear ring also can be destroyed by consumption of the gas by active star formation. Based on this argument, it has been claimed that the lifetime of a nuclear ring can be as short as 10^8 years (see also the discussion in Sect. 4.4). However, there are several galaxies with nuclear rings coexisting with inner and outer rings, both having formation time scales longer than this suggested lifetime (Buta & Combes 1996). Possible explanations for this discrepancy are accretion of gas from a small companion galaxy or recycled gas from the stellar component.

Although we have included a process that randomly changes colliding gas particles into collisionless test particles (this method was actually adopted to avoid excessive cpu-time consumption in giant gas clumps formed in the centres due to inflow in a few of the models), our usual parameter choice makes this process effective only in timescales of gigayears. The result of this process can be seen for example in the erosion of the nuclear ring of models A1.75 and A2.25 (see Fig. 13).

Most nuclear rings in simulations shrink during their early evolution. Similar behaviour was seen in the standard model of Piner et al. (1995). There are also models where shrinking can take place later. An extreme example of this is the nuclear ring in model C1.75, shown in the last row of Fig. 13: the nuclear ring finally sinks into the centre. In this case the shrinking of the nuclear ring is not due to x_2-orbits becoming unstable. This is shown by the orbit intergration of collisionless test particles. Furthermore, because changing the size or the initial distribution of gas particles can make the nuclear ring stable, it is possible that the sticky particle method has met its limits in this high density environment. There are some galaxies (Combes et al. 1992; Buta et al. 1995b) where the gas or dust component of the nuclear ring is located inside the stellar component and it has been suggested that these rings could be shrinking. It is unclear whether the shrinking of the nuclear rings in our simulations has something to do with these observed cases.

It has been suggested that the constancy of the pattern speed of the bar is necessary for the ring formation (Buta & Combes 1996) and that galaxies where the bar slows down fast could not have resonance rings. However, our results show that fairly large slow-down rates can be tolerated. For example, in model C1.75 the pattern speed of the bar decreases about 40% during the first gigayear after the bar formation. At the same time, the inner ring survives and the outer pseudoring forms. During the last 13 gigayears of this simulation, the bar pattern speed further decreases by 30%, half of which happens during the first two gigayears. While this happens, the OLR moves outwards by about 30%, which corresponds closely to the change in the size of the outer ring. However, note that the pattern speed change is much smaller during one bar rotation period, ranging from 5% by $T = 2$ Gyr to 0.5% by the end of the simulation. Larger pattern speed decreases can be present in 3D-simulations with a self-consistent halo component (Debattista & Sellwood 1998).

4.3. Miscellaneous cases

The existence of clearly misaligned ring structures, like in ESO 565-11 (Buta et al. 1995b), can at least in a few cases be explained by multiple modes present in the disks of these systems. An example of this is model B2.25. Four higher resolu-

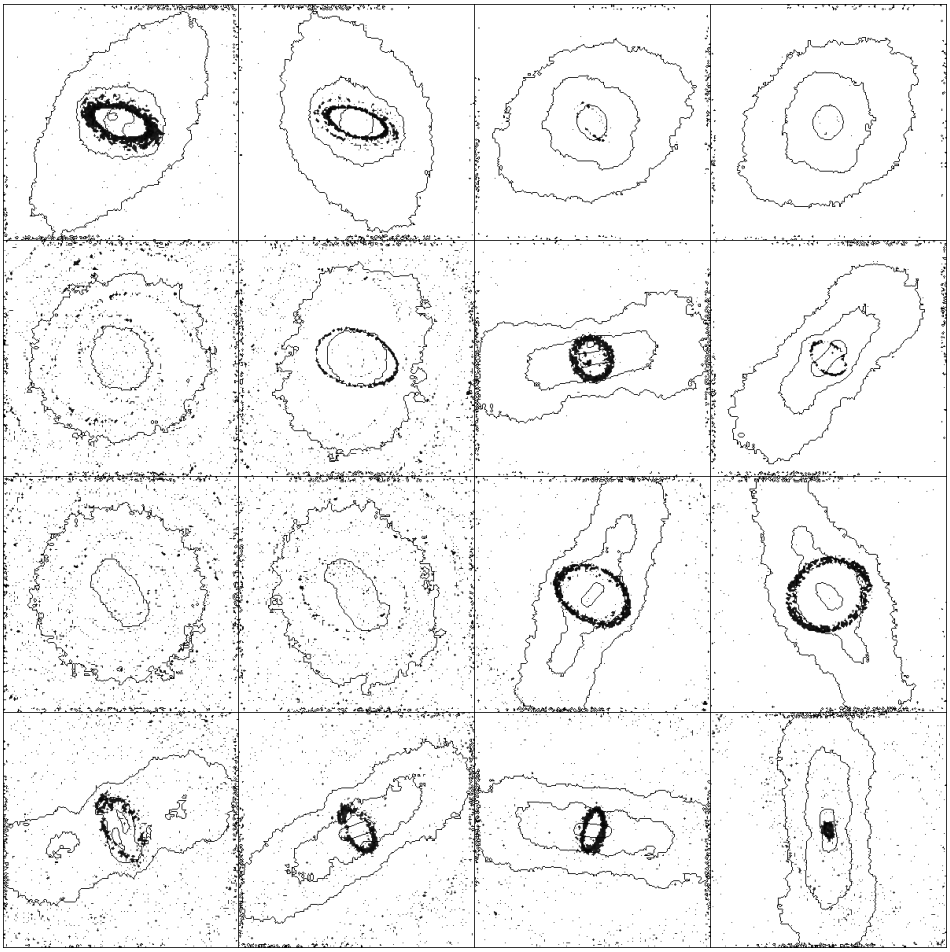

Fig. 13. Gallery of nuclear rings in models A1.75, A2.25, B2.25 and C1.75. The gas particle distribution is plotted over isodensity contours of the stellar distribution. The shown timesteps are the same as in the figures showing the large scale morphological evolution of these models, except in model C1.75, where the evolution is shown in time steps T = 1.125, 1.375, 1.625 and 1.875 Gyr. The width of the frames is 6 kpc. The nuclear rings in models A1.75 and A2.25 disappear because the high collision frequency leads to transformation of gas particles to collisionless test particles (see text).

tion frames of its evolution are shown in Fig. 14. It can be seen clearly that the relative position angle of the inner ring to the bar changes constantly. The reconstructed modes in corresponding timesteps are shown in Fig. 15. The reason for the misalignment is that the inner ring is evidently strongly affected by the mode with a lower pattern speed than the bar. In the amplitude spectrum of the gas component in the ring region, the signal is stronger in the lower pattern speed. The shape of the inner ring seems to vary with a period equal to relative period of the two modes. Maciejewski & Sparke (2000) introduced a concept of loop orbits, which exhibit a similar behaviour in their two-barred model. This concept could be useful also with nuclear and sometimes even with outer rings. Although Buta et al. (1999b) modelled ESO 565-11 with a rigidly rotating single pattern speed potential, which was derived from near-IR observations, we believe that the presence of two different modes is a more natural solution. Misaligned inner rings are very rare, only a few clear cases are known. This does not disagree with our results: model B2.25 is the only example that we have found among the approximately one hundred models we have made.

There are also galaxies which have rings but do not have a bar. It is possible that the bar has been destroyed by the inflow of gas to the nuclear region (e.g. Friedli & Benz 1993; Norman et al. 1996). However, note that in model A2.5 the oval disappears even without the effect of a massive gas component, and circular rings remain. Another possible reason for the existence of non-barred galaxies with rings is that the resonances are induced by a weak oval component (like in model A2.5) which can be hard to observe. Also, a spiral potential can form a ring, as is shown in Fig. 14 of Salo et al. (1999). This potential, which was derived from near-IR observations of IC 4214 (Buta et al. 1999a), was assumed to rotate rigidly. However, it has been suggested that in non-barred galaxies the spiral structures are formed by transient, but recurrent, patterns (Sellwood & Carlberg 1984). This view of a nonsteady spiral structure in non-barred galaxies lead Buta & Combes (1996) to consider the gravity torque of the spiral structure too inefficient to cause ring formation.

Buta and Combes' conclusion seems to be too strict, because the strongest ring structure of model C2.5, where the disk is so hot that formation of a major bar component never appears, is related to the spiral mode. The gas distribution and the contours of the restored $m = 2$ mode, with a spiral shape, at T = 6.25 are shown in Fig. 16. The inner Lindblad resonance radius of the spiral mode is also shown and the position of the ring nicely coincides with it. Although the outer Lindblad resonance of the nuclear bar is also rather close, the strength of the nuclear mode is very weak at this radius and the amplitude spectrum of the gas component clearly shows that the gas ring has the same pattern

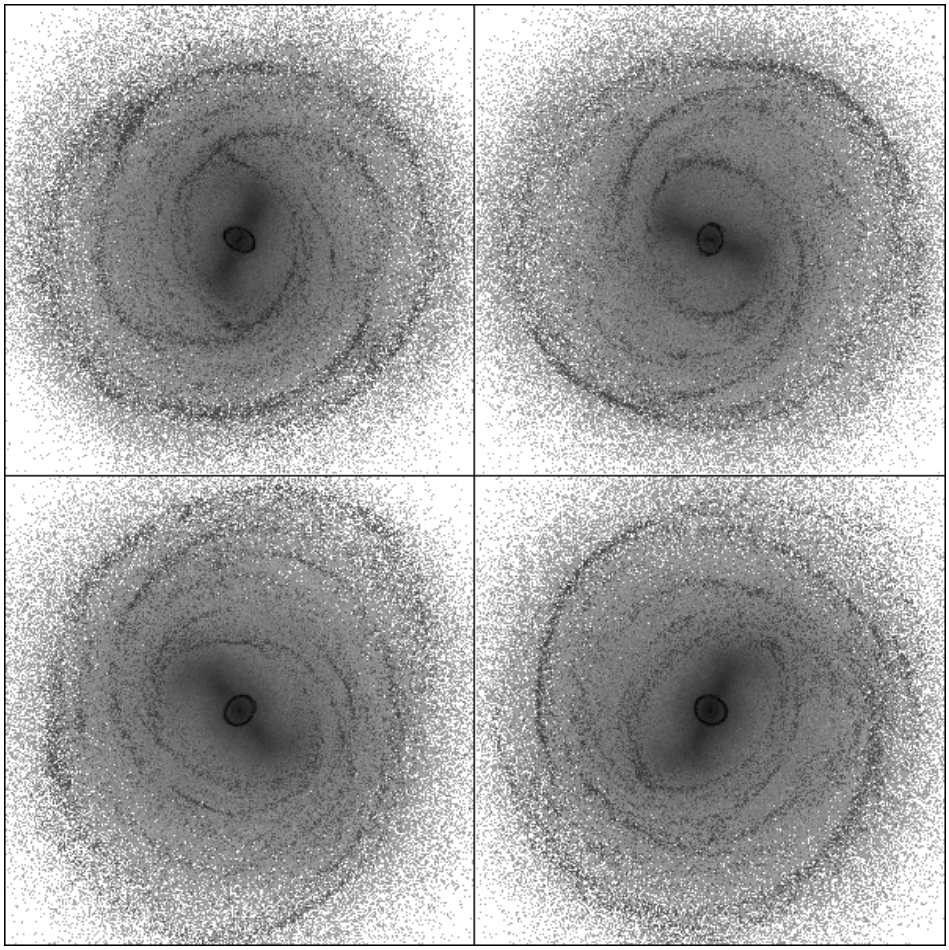

Fig. 14. The evolution of the misaligned inner ring in model B2.25. The timesteps shown are 10.0. 11.25, 12.5 and 13.75 Gyr. The width of the frames is 36 kpc.

speed as the spiral component. Thus this ring is a nuclear ring although its size is typical of inner rings. Weak innermost ring structures seen in Fig. 16 are related to the nuclear bar. This simulation shows that a spiral mode also can form a ring, at least if it is long lasting and its pattern speed is almost constant, as in this model. Furthermore, as we discussed in the previous subsection, the spiral modes often have a strong contribution in the amplitude spectra of the outer rings.

In many simulations with rigid bar potentials, the regions around Lagrange points L_4 and L_5, near the minor axis of the bar, are populated by gas particles which follow the so called banana orbits. In real galaxies, this region is usually rather empty. The situation is very similar in self-consistent simulations: such structures are very rare (something like this can be seen in the later phases of model C2.25). When the amplitude of the bar increases, this region also usually becomes empty in the analytical simulations. It is unclear why such features are not observed in galaxies with weak bars. One possibility is that in these systems this region is dominated or interfered with by a slower spiral mode. However, there is one possible exception, NGC 4579 (see e.g. the second generation images of the STScI Digitized Sky Survey), where the morphology resembles our simulations with features near the Lagrangian points.

4.4. Limitations of our modelling approach

Some of our simulations have very sharp features in the gas component. This is largely related to the level of velocity dispersion of the gas component: in models with the sharpest features, the average radial velocity dispersion, $\sigma_{\rm R}$, is about 4 kms^{-1}, whereas in models with more "fuzzy" features $\sigma_{\rm R}$ is close to 10 kms^{-1}. Furthermore, during the evolution of an individual model, the change in the sharpness of the features is usually accompanied by a change in the velocity dispersion. For example, models where a bar forms quickly, e.g. model C1.25, can have $\sigma_{\rm R}$ close to 20 kms^{-1} during the early evolution, but later the velocity dispersion becomes much lower. At the same time, the sharpness of the morphological features increases. Inspired by these trends, we have tested the effect of gas velocity dispersion on an individual model. We performed these tests by running modified versions of model C2.25, that contains all the ring types and much small scale structure in the gas component.

The energy input by stellar winds and supernovae can increase the velocity dispersion of the gas component. We modelled this by randomly forming massless "OB-particles" in collisions. These particles explode after 20 million years and give velocity pushes $v_{\rm SN}$ to gas particles nearer than a given radius $r_{\rm SN}$. A similar method was used by Noguchi (1988). Also, more elaborate schemes have been constructed (e.g. Elmegreen

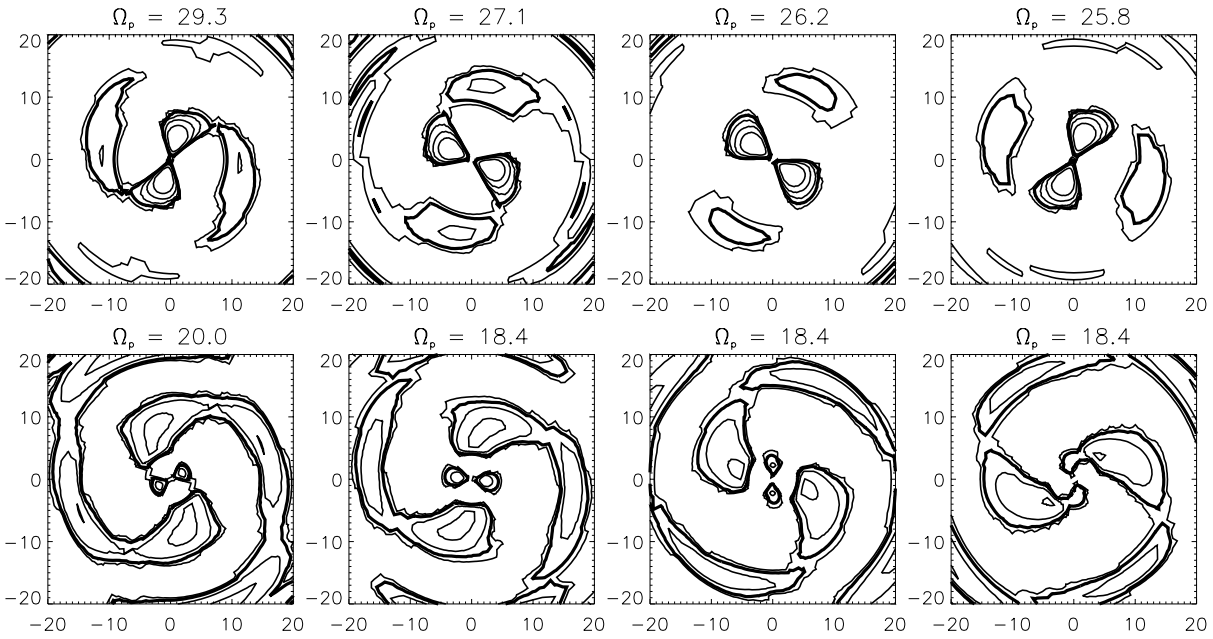

Fig. 15. A sequence showing the isodensity contours of reconstructed bar (top row) and spiral (bottom row) modes of model B2.25, which has a misaligned inner ring. The timesteps are the same as in Fig. 14.

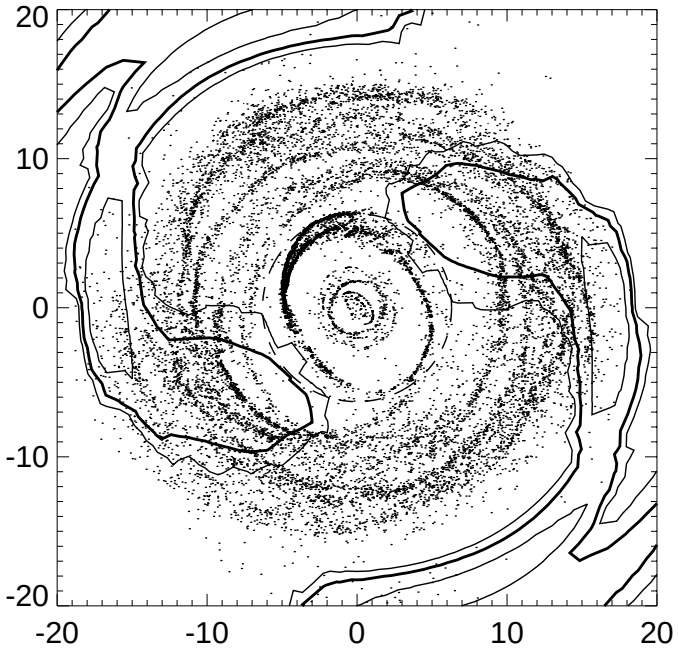

Fig. 16. The gas distribution of model C2.5 at $T = 6.25$ Gyr and the $m = 2$ spiral mode that supports a ring in its inner Lindblad resonance (shown as a dashed line). The contour levels of the mode are the same as in the figures showing the amplitude spectra.

& Thomasson 1993; Heller & Shlosman 1994; Friedli & Benz 1995). We made simulations of mass model C2.25 varying the probability of OB-particle formation in collisions ($p_{\rm OB}$ is 0.005 or 0.1) and the effective radius of the explosion (30, 150, or 375 pc). The velocity impact given by a supernova is about 15 kms^{-1}, or about 7% of the circular velocity in the peak of the rotation curve.

The effect of the supernova explosions is strongest where the collision frequency is very high, i.e. in nuclear rings. The increased velocity dispersion makes the nuclear rings wider, or if $p_{\rm OB}$ and $r_{\rm SN}$ are large enough, the ring can become unstable and collapse. In the outer disk, the increased velocity dispersion makes features less sharp. Adopting a sufficiently high probability of OB-particle formation destroys practically all the fine structure in the gas component (see Fig. 17). Interestingly, Friedli & Benz (1995) determine the upper limit for the energy injected to the gaseous component by requiring that the formation of spiral arms and rings be possible. Although our tests were done with a very crude method and rather arbitrary parameters, they show that the effect of supernovae on rings and other features can be considerable.

We also tested the effect of the coefficient of restitution α by repeating the model C2.25 with α ranging from our standard value 0.0 to 0.7. Adopting higher values of α causes the features to be more diffuse, but to avoid the formation of sharp features, the model requires $\alpha \geq 0.5$ (see Fig. 17). This agrees well with Noguchi (1999; see also Hänninen & Salo 1994, Fig. 3 for the effect of α on the sharpness of ILR resonance features on planetary ring simulations). As can be seen from Fig. 17, the inclusion of supernovae has a rather similar effect to the adopting of a higher value of the coefficient of restitution. In both test series, most of the morphological changes happen continuously, and the large scale morphology is essentially similar inside a wide range of parameters. When the velocity dispersion is high, the formation of small-scale structure is inhibited in both series, and the formation of a nuclear ring is delayed or the ring can even become unstable.

The gas component is massless in our simulations. The inclusion of the gas mass would change the stability properties

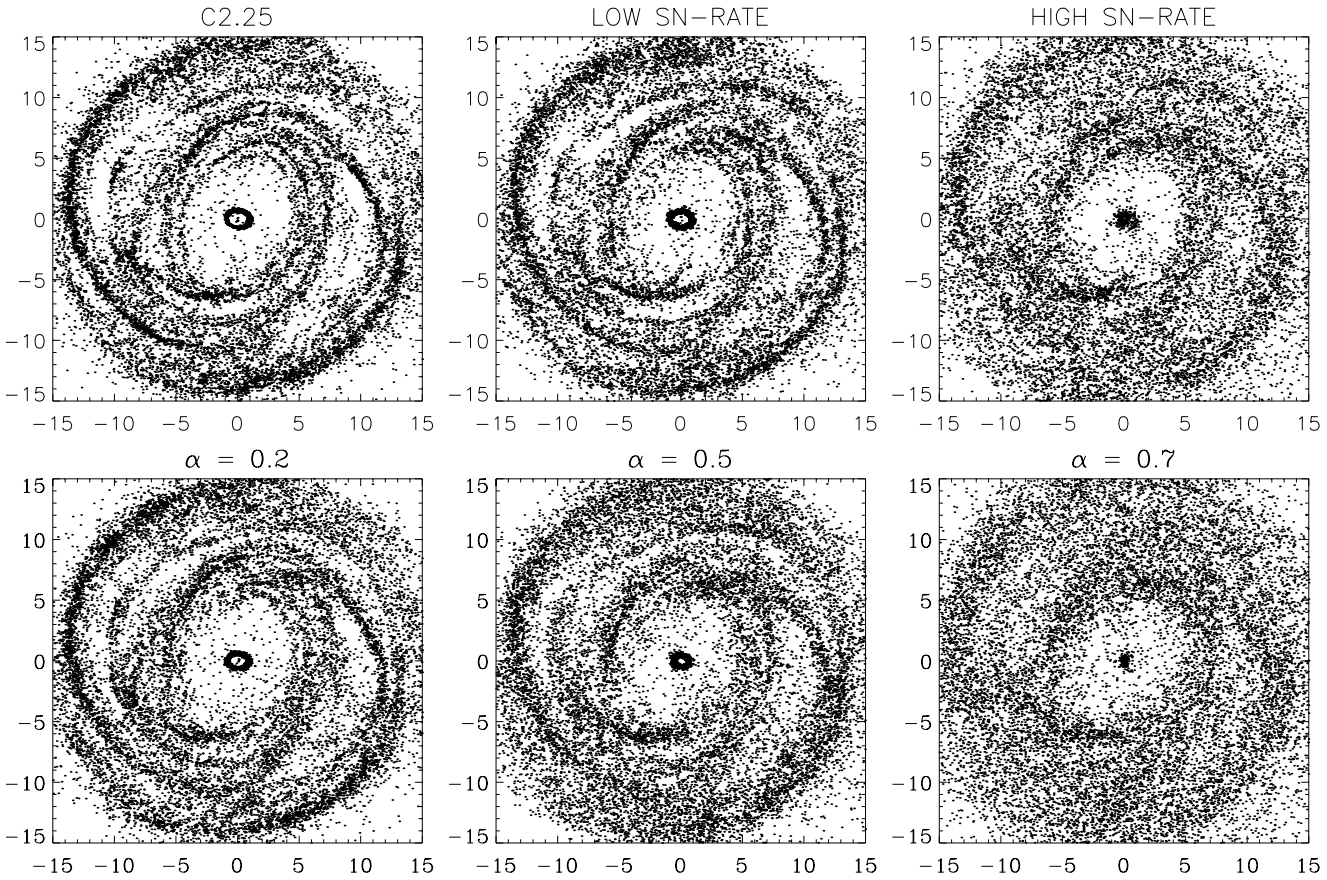

Fig. 17. The effect of the gas velocity dispersion. The top row shows model C2.25 at $T = 5.0$ Gyr, and otherwise similar models with supernova explosions with $r_{\rm SN} = 150\,pc$ included ($p_{\rm OB}$ 0.005 or 0.1). The bottom row shows C2.25 but with different values of the coefficient of restitution (the original case C2.25 has α = 0). The average radial velocity dispersion are 6.9, 7.6 and 11.3 kms^{-1} for the top row, and 7.2, 9.2 and 14.5 kms^{-1} for the bottom row.

of the disk (e.g. Bertin & Romeo 1988; Shlosman & Noguchi 1993). Sellwood & Carlberg (1984) modelled the accretion process by adding stars to a self-gravitating disk on circular orbits, imitating the cooling effect of the young stellar population formed from the accreted gas. They suggested that barred galaxies would be systems with a high initial accretion rate. The opposite conclusion was found by Noguchi (1996). In his numerical model the high gas accretion rate led to formation of massive gas clumps, which scattered the disk stars and made the system stable against bar formation. Another gas related process is the bar-induced gas inflow towards nucleus, which can change the gravitational potential so that the bar would be destroyed, or at least become weaker (Friedli & Benz 1993; Norman et al. 1996).

Three-dimensional simulations of barred galaxies (e.g. Combes & Sanders 1981; Raha et al. 1991) have shown that a bar can become considerably thicker than the original stellar disk, forming a box-like or peanut-shaped bulge component. One would expect that this process would decrease the strength of the non-axisymmetric perturbation, at least in the bar area. In single-mode systems with a very strong bar, this weakening of the non-axisymmetric perturbation could make x_2 orbits stable, and thus lead to the formation of a nuclear ring.

5. Conclusions

Although studies applying rigidly rotating bar potentials have shed light on the formation of rings in the disks of galaxies, self-consisted simulations provide valuable complementary information:

1) Our results support the standard hypothesis that links rings to resonances, which in most cases are induced by the bar component. More specifically, the outer rings are usually related to the outer Lindblad resonance, the inner rings to the inner 4/1-resonance and the nuclear rings to the inner Lindblad resonance. Alternatively, nuclear rings can be related to nuclear modes with higher pattern speed than that of the main bar.
2) The systems with very strong bars can lack nuclear and sometimes also inner rings. The nuclear rings can be absent also in systems where the bar rotates so fast that it does not have an inner Lindblad resonance. It is also possible that a starburst related to a nuclear rings consumes so much gas that the ring dissolves.
3) There are several ways to explain the absence of outer rings in barred galaxies. The age of the bar may be lesser than the timescale of outer ring formation, and thus systems with recently formed bars would naturally miss an outer ring. It is also possible, as suggested by Elmegreen et al. (1992), that interac-

tions with other galaxies can destroy outer rings. However, the presence of the outer spiral mode with a lower pattern speed than that of the bar could not prevent outer ring formation. The situation is the same with the deceleration of the bar pattern speed and the corresponding change in the resonance positions: an existing ring reacts to the increasing outer Lindblad resonance radius by becoming larger.

4) Outer pseudorings can form also in the self-gravitating stellar component. These rings are much broader than the gaseous rings and can exhibit different morphology.

5) In cases with several modes near the OLR of the bar, the evolution can be almost cyclic: the morphology of the outer structure changes between different outer ring subclasses and occasionally there is not a clear ring or a pseudoring.

6) Systems where the orientations or the sizes of the rings are different to the normal values can be explained by assuming the presence of several modes with different pattern speeds. This is the case in one of our models, where the inner ring is misaligned with the bar. Such features do not form in models with a single analytical bar potential, but can be present in self-consistent simulations.

7) In addition to bars, rings can be formed by ovals. Also, spiral modes can produce rings if their lifetimes are long enough and their pattern speeds relatively constant. It is possible that at least part of the rings in non-barred galaxies are formed this way.

8) Some rings in non-barred galaxies can be formed by bars or ovals, which are later dissolved. In one of our simulations, this happened even without gas inflow or an interaction with another galaxy.

Our models have two major limitations: they are two-dimensional and the modelling of the gas component is very simplified. We intend to make improvements in both aspects in our forthcoming studies.

Acknowledgements. We want to thank referee, F. Combes, for her comments that helped to improve the manuscript. We are also grateful to R. Buta for his comments. Financial support from the Finnish Graduate School of Astronomy and Space Physics and the Wihuri Foundation is acknowledged. We found the STScI Digitized Sky Survey very useful in our study. The Digitized Sky Surveys were produced at the Space Telescope Science Institute under U.S. Government grant NAG W-2166. The images of these surveys are based on photographic data obtained using the Oschin Schmidt Telescope on Palomar Mountain and the UK Schmidt Telescope. The plates were processed into the present compressed digital form with the permission of these institutions. The National Geographic Society - Palomar Observatory Sky Atlas (POSS-I) was made by the California Institute of Technology with grants from the National Geographic Society. The Second Palomar Observatory Sky Survey (POSS-II) was made by the California Institute of Technology with funds from the National Science Foundation, the National Geographic Society, the Sloan Foundation, the Samuel Oschin Foundation, and the Eastman Kodak Corporation. The Oschin Schmidt Telescope is operated by the California Institute of Technology and Palomar Observatory. The UK Schmidt Telescope was operated by the Royal Observatory Edinburgh, with funding from the UK Science and Engineering Research Council (later the UK Particle Physics and Astronomy Research Council), until 1988 June, and thereafter by the Anglo-Australian Observatory. The blue plates of the southern Sky Atlas and its Equatorial Extension (together known as the SERC-J), as well as the Equatorial Red (ER), and the Second Epoch [red] Survey (SES) were all taken with the UK Schmidt. Supplemental funding for sky-survey work at the ST ScI is provided by the European Southern Observatory.

References

Athanassoula E., 1996, in: Buta R., Crocker D.A., Elmegreen B.G. (eds.) Barred Galaxies. IAU Colloquium 157, ASP Conf. Series 91, p. 309
Athanassoula E., Bosma A., 1985, ARA&A 23, 147
Athanassoula E., Sellwood J.A., 1986, MNRAS 221, 213
Bertin G., Romeo A.B., 1988, A&A 195, 105
Buta R., 1995, ApJS 96, 39
Buta R., Combes F., 1996, Fundamentals of Cosmic Physics 17, 95
Buta R., Combes F., 2000, In: Combes F., Mamon G., Charmandaris V. (eds.) Dynamics of Galaxies: From the Early Universe to the Present. ASP Conf. Series 197, p. 11
Buta R., Crocker D.A., 1991, AJ 102, 1715
Buta R., Crocker D.A., 1993, AJ 105, 1344
Buta R., van Driel W., Combes F., et al., 1995a, ApJ 450, 593
Buta R., Purcell G.B., Crocker D.A., 1995b, AJ 110, 1588
Buta R., Purcell G.B., Cobb M.L., et al., 1999a, AJ 117, 778
Buta R., Crocker D.A., Byrd G.G., 1999b, AJ 118, 2071
Byrd G., Rautiainen P., Salo H., Buta R., Crocker D.A., 1994, AJ 108, 476
Combes F., Gerin M., 1985, A&A 150, 327
Combes F., Gerin M., Nakai N., Kawabe R., Shaw M.A., 1992, A&A 259, 27
Combes F., Sanders R.H., 1981, A&A 96, 164
Contopoulos G., Grosbøl P., 1989, A&AR 1, 261
Crocker D.A., Buta R., 1993, BAAS 25, 1416
Crocker D.A., Baugus P.D., Buta R., 1996, ApJS 105, 353
Debattista V.P., Sellwood J.A., 1998, ApJ 493, L5
Debattista V.P., Sellwood J.A., 2000, preprint: astro-ph/0006275
Elmegreen B.G., Thomasson M., 1993, A&A 272, 37
Elmegreen D.M., Elmegreen B.G., Combes F., Bellin A.D., 1992, A&A 257, 17
Elmegreen D.M., Elmegreen B.G., Chromey F.R., Hasselbacher D.A., 1996, ApJ 469, 131
Elmegreen D.M., Chromey F.R., Warren A.R., 1998, AJ 116, 2834
Friedli D., Benz W., 1993, A&A 268, 65
Friedli D., Benz W., 1995, A&A 301, 649
Friedli D., Martinet L., 1993, A&A 277, 27
Hänninen J., Salo H., 1994, Icarus 97, 228
Heller C.H., Shlosman I., 1994, ApJ 424, 84
Hunter J.H., Ball R., Huntley J.M., England M.N., Gottesman S.T., 1988, ApJ 324, 721
Lindblad P.A.B., Lindblad P.O., Athanassoula E., 1996, A&A 313, 65
Maciejewski W., Sparke L.S. 2000, MNRAS 313, 745
Masset F., Tagger M., 1997, A&A 322, 442
Noguchi M., 1988, A&A 203, 259
Noguchi M., 1996, ApJ 469, 605
Noguchi M., 1999, ApJ 514, 77
Norman C.A., Sellwood J.A., Hasan H., 1996, ApJ 462, 114
Piner B.G., Stone J.M., Teuben P.J., 1995, ApJ 449, 508
Raha N., Sellwood J.A., James R.A., Kahn F.D., 1991, Nat 352, 411
Rautiainen P., Salo H., 1999, A&A 348, 737
Romeo A.B., 1994, A&A 286, 799
Salo H., 1991, A&A 243, 118

Salo H., Rautiainen P., Buta R., et al., 1999, AJ 117, 792
Schwarz M.P., 1981, ApJ 247, 77
Sellwood J.A., Carlberg R.G., 1984, ApJ 282, 61
Sellwood J.A., Sparke L.S., 1988, MNRAS 231, 25p
Sellwood J.A., Wilkinson A., 1993, Reports on Progress in Physics 56, 173
Shlosman I., Noguchi M., 1993, ApJ 414, 474
Tagger M., Sygnet J.F., Athanassoula E., Pellat R., 1987, ApJ 318, L43
Toomre A., 1964, ApJ 139, 1217
Verdes-Montenegro L., Bosma A., Athanassoula E., 1995, A&A 300, 65
Zaritsky D., Lo K.Y., 1986, ApJ 303, 66